NOISE REDUCTION OF TUNABLE RESISTIVE PULSE SENSING FOR IMPROVED

EXTRACELLULAR VESICLES PROFILING IN CANCER DETECTION

A Thesis
Submitted to the Graduate Faculty
of the
North Dakota State University
of Agriculture and Applied Science

By

Nega Ejjigu

In Partial Fulfillment of the Requirements
for the Degree of
MASTER OF SCIENCE

Major Program:
Biomedical Engineering

April 2022

Fargo, North Dakota

North Dakota State University
Graduate School

Title

NOISE REDUCTION OF TUNABLE RESISTIVE PULSE SENSING
FOR IMPROVED EXTRACELLULAR VESICLES PROFILING IN
CANCER DETECTION

By

Nega Ejjigu

The Supervisory Committee certifies that this ***disquisition*** complies with North Dakota

State University's regulations and meets the accepted standards for the degree of

MASTER OF SCIENCE

SUPERVISORY COMMITTEE:

Dr. Dali Sun

Chair

Dr. Bo Liang

Dr. Danling Wang

Approved:

April 8, 2022	Dr. Benjamin Braaten
Date	Department Chair

ABSTRACT

EVs have much potential as sensitive, novel biomarkers because they represent the status of their cells of origin and can be used to detect cancer earlier than alternative biomarkers. The size of EVs can be determined by tunable resistive pulse sensing (TRPS). However, TRPS is susceptible to environmental noise, including mechanical and electrical noise that limits detection precision. To overcome these noises, an external device was designed, guided by flow simulations, to reduce noises that interfere with TRPS measurements. Both mechanical and electrical environmental noise reductions were observed after using the shield. The study also validated the noise reduction function of the shield by quantifying EVs from different cell origins. This study demonstrates innovation in designing shielding enclosures using composite material to improve the sensitivity of emerging tunable resistive pulse technology to quantify EVs below 200 nm, which is challenging using traditional quantification methods.

ACKNOWLEDGMENTS

DEDICATION

Dedicated to my mother Tiruaynet Dires who supported me through my high school as a single

mother.

TABLE OF CONTENTS

LIST OF TABLES

LIST OF FIGURES

1. BACKGROUND

Currently, EVs are being investigated for their role in cell signaling and as a potential biomarker to diagnose diseases. "EV" is a general umbrella term typically used as a generic reference to secreted vesicles. These vesicles have a wide variety of names such as ectosomes, microparticles, microvesicles, exosomes, and oncosomes[1]. In recent years, researchers have investigated the role of EVs in immune response, homeostasis, angiogenesis, thrombosis, tumor growth, and metastasis[2]–[8]. Although the pathological role of EVs has been intensively studied, their role in maintaining homeostasis and regulating physiological functions is less studied[9]. In the 1980s, exosomes were considered organelles, and their release was considered a simple waste disposal mechanism[10], [11]. In the following years, exosomes, a subtype of EVs were found to be vesicles that are secreted by cells and released by cells into extracellular space. Currently, the pathophysiological role of exosomes in cancer-related diseases is being investigated. Over the past few years, research on different subtypes of EVs including exosomes has gained attention due to their potential for diagnosis[12].

EVs containing proteins, nucleic acids, and lipids have seen an exponential increase in their use in biomarker discovery. Biomarkers are indicators of normal physiological processes, disease stage, or response to treatment[13]. Because of their minimal invasiveness, and their availability in biological fluids, exosomes have more advantages as biomarkers when compared to diagnosis that involves tissue biopsies. Information from the more robust lipid content of exosomes has the potential for early detection of cancer disease. Understanding the colloidal properties of EVs is crucial for effectively using EVs for clinical applications such as diagnostics, therapeutics, and devices[14]. Exosomes contain lipids that play a role in biological activity, transport biologically active molecules between cells, and affect physiological

1

functions. In addition, exosomes have the potential for drug delivery and cellular function involving exocytosis[15]. Exosomes are found in circulation and contain cell-derived bioactive molecules (e.g., mRNAs, miRNAs, and other non-coding RNAs)[16]. The study of exosomal contents includes the quantification of exRNA[17]. Investigation of exosome content, such as protein, lipid, and glycomic content, has been the subject of recent research. Other characteristics of exosomes that require further analysis include refractive index[18] In the field of nanomedicine, information about the content of exosomes has the potential to represent the state of their parent cells, which can aid in diagnosis[19]. Because the informational content of exosomes has the potential to suggest the state of origin of their parental cells, they have caught the attention of researchers in this new field of study. Information from distinct EV species provides unique signatures which are typical for EV populations from different cell origins and help to regulate stages of disease pathways. Research on EVs can help find biomarkers in the early diagnosis of disease, as they have the potential to differentiate disease conditions from health conditions.

Pathophysiological studies have shown that EVs are elevated in disease states including ovarian cancer, melanoma, kidney cancer, pancreatic cancer, glioblastoma, cardiovascular disease, malaria, diabetes, systemic lupus erythematosus, lupus erythematosus, rheumatoid arthritis, and renal failure[15], [19]–[27]. The connection between secretion of tumor-derived microvesicles and disease stage has been reported for the first time in ovarian cancer disease. In addition, studies have shown that the staging of cancer diseases has a link with the secretion of exosomes in cells. Exosomes also act as a molecular cargo carrier and contribute to a microenvironment that promotes the survival of cancer cells[28]. Previous studies have shown that the administration of cancerous exosomes to the pancreas of mice elevated metastasis[29].

Characterization of heterogeneous subpopulations of EVs is crucial to use as biomarkers. Comprehensive characterization of EVs requires investigation of their size, zeta potential, and their exosome contents. When EV populations are similar in a particularly characteristic feature, further studies such as surface charge, hydrophobicity, and capacity to transfer hydrogen can be studied to differentiate them. The quantification of EVs relies on the availability of technologies and high throughput methods[30]. Heterogeneity of exosomes based on their sizes has been studied to distinguish exosome subpopulations Classification of EVs based on their sizes are exosomes, microvesicles, and apoptotic bodies. Exosomes range in size from 30-200 nm, microvesicles range from 100-1000 nm, and apoptotic bodies exceed 1000 nm[31]. Moreover, exosome subpopulations are classified as large exosomes for the size of vesicles ranging between 90-120 nm, small exosomes for size ranges between 60-80 nm, and non-membranous nanoparticles for vesicle size of approximately 35 nm. Because of their small size, characterization of exosomes such as structural properties and heterogeneity are not well analyzed. Accurate isolation and quantification of such small nanosized exosomes are required for biomarker discovery.

Potential sources of EVs are cell culture medium, blood, urine, and saliva [32]–[37]. The ability to isolate exosomes from biological fluids facilitates the study of EVs as potential biomarkers. Since exosomes are smaller in size, their isolation method is challenging[38]. Most conventional EV isolation methods rely on the physical characteristics of vesicles such as size and density. As most size-based EV isolation methods are challenging for small exosomes, other isolation techniques are evolving. Hence, finding an accurate isolation method for the analysis of exosomes is critical in the evolving field of EVs study.

Exosome isolation methods include ultracentrifugation, ultrafiltration, immunoaffinity (IF) capture using magnetic beads, microfluidics, and size exclusion chromatography. To explore the potential of EVs as biomarkers, isolation of small EVs from large vesicles is crucial. Currently, the most used exosome isolation method is ultracentrifugation[39]. The first step of the conventional isolation method requires 30 minutes of low-speed differential centrifugation at about 10000g. This first step removes dead cells as well as large apoptotic debris. The second process requires ultracentrifugation at speeds up to about 100,000g for about 2-3 hours to remove larger vesicles and debris. However, isolation using sequences of ultracentrifugation method is time-consuming, requires a large volume of the analyte, the equipment is not portable, and is comparatively expensive. Also, the ultracentrifugation method requires multiple washing steps, which will result in the inevitable loss of some EV populations. Hence, both exosome yield recovery and purity using this sequence of centrifugation are low[40], [41]. The isolation can be performed using individual methods or using a combination of different methods. To enhance the isolation technique, some protocols apply microfiltration in the first centrifugation process to reduce the time required for isolation as well as to obtain more purified EVs. In this microfiltration approach, a nano-membrane concentrator helps to enrich exosomal contents. In addition, size exclusion chromatography after the ultracentrifugation step could provide more purified EVs. The principle of EVs isolation in size-exclusion chromatography relies on the physical dimensions of vesicles. Recently, Merchant et al. [42] demonstrated a size-exclusion-based microfiltration technique using low protein binding filters. Although there are methods for EVs isolation, the lack of standardization is a problem. This variation in the isolation protocol results inconsistent results for the yield recovery of EVs. The inconsistency can be attributed to the difference in viscosity of EVs.

Quantification of EVs requires repeatable and effective isolation methods. Challenges in exosome isolation methods have given rise to advanced emerging technologies, including microfluidic devices, magnetic nanomaterials, precipitation techniques, and antibody-coated magnetic beads. Since EVs consist of specific surface biomarkers, they can be isolated via immunoprecipitation methods utilizing antibody-conjugated magnetic beads that can then be analyzed with proteomic methods to study their contents. In the magnetic beads-based isolation method, anti-EpCAM magnetic beads can capture cancerous EpCAM EVs. This isolation method helps to discriminate sub-populations of EVs based on their protein contents. Although the antibody-coated magnetic bead separation method is promising, it yields EVs in small volumes.

Several biotechnological companies are developing different EVs isolation methods. A rapid and uncomplicated isolation method for biofluids is important for higher EV yields. Microfluidic filtration provides a more purified exosome yield and allows the investigation of biofluid flow in microchannels. Biofluids flowing through microchannels are subjected to frictional rather than kinetic forces to control the separation. In the microfluidic separation method, nanoporous membranes can separate vesicles from blood samples and allows integration with microfluidic chips, where more purified EVs can be obtained by applying DC electrophoresis to drive particles through the filters. An experimental demonstration of this microfluidic filtration was carried out by Ryan et al[41]. In this demonstration, EVs from mouse blood was isolated using a porous polymer monolith membrane as a size-exclusion filter technique. Microfluidic devices reduce material costs and offer the potential to analyze small volumes of analytes with high throughput. Moreover, microfluidic cards allow the characterization of small-sized microvesicles for high throughput. In contrast to antibody-coated

magnetic bead separation, microfluidic isolation requires only one step capture from serum samples, and this enhances the isolation of EVs from contaminating proteins. Also, the microfluidic approach reduces the more laborious sequence of ultracentrifugation steps that may potentially damage the vesicles. Hence, the isolation of smaller-sized EVs from blood using a microfluidic filtration system provides intact EVs. Also, Exoquick^{TM} is another isolation method to overcome the challenges of EV isolation. In this method, the mixture from the Exoquick^{TM} kit can be added to the target analyte, and the EVs are allowed to settle overnight in the incubator.

Although EVs have clinical potential for early diagnosis, the lack of sensitive analytical systems for EV analysis created barriers to clinical translation. Translational validation of EVs as biomarkers requires the study of correlations between disease states and specific EVs biomarkers. To accomplish this critical validation step, the availability of technologies that can rapidly characterize EVs is critical. However, quantification of exosomes with low refractive indices, polydisperse, and heterogeneous in size is challenging. Furthermore, quantifying exosomes is challenging due to their low mass and high particle number. Small EVs with a diameter of 150 nm, contains about 10,000 nucleotides of different nucleic acids and up to 100 proteins[43]. To advance improvement in characterization methods of exosome subpopulations, understanding the advantage and limitations of each technology is important. Also, developing standards for exosome quantification methods is required for comparative analysis[44]. Developing standards for EVs quantification methods facilitates the translation of exosomal biomarkers for clinical settings. Webber et al. pointed out another way for normalization using total protein quantifications[45]. However, this method also requires normalization for each source of EVs.

Particle size determination is essential for analyzing biomolecular analytes[46]. One of the important criteria for identifying cell-derived EVs is using their size[47]. In vesicles size determination, it is assumed that vesicles are spherical in their native state, and thus size quantification is in diameter. The reproducibility, sensitivity, and dynamic range of devices that can quantify exosomes is an area that requires further research. Current particle size quantification methods use independently NIST-certified calibration particles. However, there is a lack of concentration standards to calibrate exosome counting devices. There are different conventional ways to quantify the size of EVs, but there is a need for a fast, sensitive, and high-throughput method. Qualitative analysis of small EVs could be analyzed using transmission electron microscopy (TEM) and atomic force microscopy (AFM) methods. However, these methods are incapable of providing information related to the number of particles Also, size determination using the TEM method requires sample preparation procedures. The steps involve fixing the sample and dehydrating it. These sample fixing processes could potentially affect the natural morphology of EVs[48]. Other EV quantification methods include flow cytometry, ELISA, electrochemical detection, microfluidics, and dynamic light scattering[49]–[53]. Electrochemical, fluorescence, and microfluidic EVs quantification methods have been introduced to improve sensitivity. To further study the biology of small nanoscale vesicles, new technological advances that enable better isolation and characterization are required. Nanoparticle-driven biosensors are constantly being developed to meet the need for fast and convenient quantification of vesicles. Therefore, other methods such as nanoparticle tracking analyzer (NTA) and TRPS technology have emerged for EVs analysis[54]–[56].

Quantification of EVs is challenging because the sizes of many vesicles are less than 100 nm, heterogeneous in size and composition, and their refractive indices are low[57], [58].

However, the current research on exosomes requires the quantification of sizes ranging from 30 to 150 nm. The ability to characterize heterogenous exosomes is important to study their difference, investigate their content, and understand their role in physiology. The small size of exosomes is important for drug delivery as it facilitates rapid clearance by phagocytes[59]. Hence, the ability to characterize small nanoscale exosomes will contribute to the development of nucleic acid encapsulation therapy. Several studies have reported challenges in developing an analytical system that can distinguish between distinct types of EVs[60].

Coulter counters are resistive pulses sensing devices designed for the quantification of cells and colloidal particles. The first automated Coulter counter detection method principle uses impedance characteristics of the cell that passes through an orifice[61]. In 1953, Wallace Coulter demonstrated the quantification of micrometer-sized targets such as bacteria, cells, and other particles. 'Coulter counting Principle' has also been used in research settings for the measurement of air bubbles created due to dissolution. Deblois et al. were the first to apply the Coulter counting principle for size profiling of 60 nm diameters extracellular virus particles and 90 nm diameters of polymer particles[62]. More recently, Crooks et al. reported the advanced Coulter counter-resistance pulse method, which utilizes a polydimethylsiloxane membrane that contains an array of specific carbon nanotubes of about 130 nm in diameter[63].

Another version of the Coulter counting resistive pulse sensing is microfluidic resistive pulse sensing. The technology enables the analysis of samples on a lab-on-a-chip platform. Currently, a microfluidic device is being introduced for the quantification of the size and concentration of cells in a chip, and particles suspended in a buffer[64]. Microfluidic devices are related to the original cell counter devices; however, they are limited to the quantification of micrometer-sized particles[65]. Similar to TRPS, a microfluidic device uses two electrolyte-

8

filled chambers. These chambers are separated by a microscopic conduction channel. Microfluidic resistive pulse sensing quantifies the size of an analyte by detecting changes in resistance in a microchannel as particles in an electrolyte pass through it. This change in resistance appears as a resistive pulse current. The magnitude of pulsed current and its duration characterize the size, shape, concentration, and zeta potential of the target particles. Microfluidic devices have the potential to meet the demand for portable and low-cost diagnostic tools[66]. Also, microfluidic systems have simplicity and flexibility due to the availability of parts that enable troubleshooting. However, commercializing microfluidic technology require improvements on unstable cell viability in the chip. For cell quantification research, recent strategies use microfluidic chip systems in parallel with traditional cell counting methods. To fully replace the recent cytometers with the emerging microfluidic technology, advancements in analyte preparation and detection strategies are required.

Multiplexed resistive pulse sensing is the future of microfluidic resistive pulse sensing. Resistive pulse sensors with multiple apertures increase throughput in particle analysis. The multi-channel resistive pulse sensing adopts the principle of cellular telecommunication. In cellular communications, many cell phone users can communicate with each other at the same time through a base station using the same channel via Time Division Multiple Access (TDMA). Similarly, a microfluidic device replicates the same principle to multiplex the signal coming from various microfluidic channels. Then, for particle analysis, a single-data acquisition is used by reconstructing signals coming from each different channel. An experimental demonstration of this principle was first carried out by Gihoon et al.[67]. In this demonstration, the size and concentration of polystyrene beads were evaluated using an eight-channel microfluidic device. This multichannel approach is low-cost and allows quantification even in the event of a few

9

channels clogging through other available channels. This approach addresses the most challenging problem of nanopore clogging in resistive pulse sensing technology.

Nanopores are nanoscale Coulter counter devices. The nanopore fabrication applies a polyurethane membrane. The pore is tunable and punctured using a micrometer size tungsten needle. Fabrication of such elastic tunable pore is a comparatively recent technology[68]. In this TRPS technique, size quantification of colloidal particles is performed using polyurethane nanopores[69]. Nanopore fabrication technology has seen significant development over the past 10 years. This advancement in nanopore fabrication technology has brought back the use of the Coulter counter resistive pulse method for rapid particle-by-particle analysis. Since EVs possess unique electrical, optical, and magnetic properties, the past decade has seen rapid growth in developing new devices for their quantification. In addition to the quantification of EVs, nanopores can also detect proteins and DNAs[70]. The TRPS technique is one of the emerging technologies that have the potential to quantify biological fluids[69].

Recently, the qNANO device uses TRPS technology to quantify nanoparticles. Nanopore-based TRPS technology allows controlling the pore size. This technique applies macroscopic axial stretching force to the elastic membrane to improve sensitivity for quantifying a wide range of particle sizes. The device can analyze nanoparticles ranging from 40 nm to 10 μm[72]. TRPS technology applies a trans-membrane DC voltage to drive electrophoresis[73]. Applying a voltage across the membrane causes ions to drive through the nanopore and establish an ionic baseline current across the nanopore (schemed in Figure1). This particle motion prevents the flow of ionic current through the pore. This blockade causes a small resistive pulse current. The blockade current provides information to quantify the magnitude of a nanoparticle. The TRPS method uses this working principle for size analysis and determination of EV

10

concentrations. Resistive pulse sensing is most helpful for studying cellular function and uptake. This method is applicable for the quantification of biological fluids such as DNA, proteins, small biomolecules, and artificial polystyrene nanoparticles as proof-of-principle.

The TRPS technique is suitable for use in parallel with other quantification methods such as nanoparticle tracking analyzer, transmission electron microscopy, and dynamic light scattering. Light scattering detection relies on a high reflective index of scattered light and monodisperse distribution of vesicles[74]. Flow cytometry is applicable for high throughput EVs detection, but the weak scattered light from EVs with sizes less than 100 nm makes accurate quantification challenging[75]. In dynamic light scattering, the quantization principle relies on the Brownian motion of particles. Hence, this method is only applicable to the monodisperse distribution of particles. System optimization for precise quantification requires setting voltage across the nanopore, selecting the appropriate nanopore size for the target nanoparticle size, and controlling pore size by adjusting the strain. Practical challenges for nanopore-based sensors include noise, repeatability, controllability, and large-scale fabrication[76]. Nanoparticle quantification using the TRPS method is subjected to ionic current fluctuations.

System overall noise is one of the challenges in the TRPS method for the quantification of EV. Noise interferes with the magnitude of the baseline current, resulting in a deviation of the relative blockade magnitude (ratio of blockade magnitude to baseline current). This interference can cause changes in the quantification of smaller particles close to the lower limit of detection. The determination of the lower detection limit of TRPS relies on the ability to detect the minimum amplitude of the resistive pulse current signal comparable to the system's overall noise[77]. Furthermore, the ratio of particles to pore size and the path of the particles through the nanopore determine the detectable size range.

Nanopore sensors often fail to sample data when fast translocation events occur. This leads to a decrease in sensitivity due to the resistive pulse signal being cut off near the noise level. The noise current across the nanopore follows a Gaussian distribution and is defined as the root mean square (RMS) of the trans-membrane current. RMS noise current value is obtained from the standard deviation of all current measurements during translocation events[78]. Noise in the time domain mathematically can be calculated using the formula,

$$I_{\text{rms}} = \sqrt{\overline{\Delta I^2(t)}} \, ,$$

where $\Delta I(t)$ indicates the fluctuation of a small ionic current that deviates from its mean value[79], [80]. Signal to noise ratio (SNR) can be evaluated as,

$$SNR = \Delta I_{ionic} / I_{\text{rms}},$$

where ΔI_{ionic} stands for the signal current amplitude and I_{rms} indicates the magnitude of noise[81]. The upper detection limit relies on the physical size of the pore, and the lower limit relies on the electrical SNR[82]. Since the nanopore sensing method is very sensitive, external noise affects the sensor's response[83].

Reducing the influence of external noise requires a shield to be designed. A shield is an enclosure that separates two regions of space to control the path of incoming electric and magnetic waves. There are two approaches for reducing the effects of electromagnetic wave interference. The first strategy is to contain external noise by surrounding the noise source with shielding material. The other strategy, which was chosen, is to surround a measuring device with a shield. Ideally, all noise sources should be shielded but due to impracticality surrounding the device was chosen.

Shielding effectiveness is described as the capacity of shielding material to reduce the strength of an electromagnetic wave. Shielding effectiveness (total attenuation) can be measured

12

in decibels (dB). Parameters that affect shielding effectiveness are frequency of striking magnetic field, the geometry of a shield design enclosure, properties of shielding material, direction, and polarization of propagating fields.

An electromagnetic wave that strikes a metallic shield is susceptible to a loss. The first type of reflection loss occurs when the wave is partially reflected from the surface of a shield. The second absorption loss occurs when components of the wave pass through the boundary that separates two regions of space. The third loss is due to the thin shield design. This thin shield design causes the reflected electromagnetic wave to be re-reflected.

2. INTRODUCTION

Studies have shown that pancreatic cancer is the third deadliest disease in the united states. Statistical data shows patients diagnosed with pancreatic cancer have a 5-year survival rate of 9%[84]. The projected statistical model shows pancreatic cancer could potentially become the second deadliest disease in the United States by 2030[85]. Furthermore, pancreatic cancer is the only cancer disease showing an increase in mortality rate. This increase can be attributed to pancreatic cancer's lack of early diagnosis when compared to other forms of cancer.

Commonly used traditional biomarkers such as plasma metabolites, cytokines, and physical parameters are not enough to monitor stage-dependent disease. The poor prognosis of pancreatic ductal adenocarcinoma (PDAC) results in highly metastatic disease[86]. Also, PDAC is resistant to chemotherapy. Previous studies have shown that most patients receive treatment at an advanced stage of pancreatic cancer. Consequently, the poor prognosis of pancreatic cancer leads to unsuccessful treatment outcomes in the late stages of a cancer diagnosis. By early diagnosis of pancreatic cancer, the survival rate could be improved 6-fold (5-year survival rate of 41.6%), but there is no useful clinical test that can help to identify patients with early pancreatic cancer[87]. Therefore, there is a need to find sensitive biomarkers with the potential for early detection of cancer. To address this need, researchers have been collaborating on finding biomarkers that can aid the early diagnosis of pancreatic cancer.

Small extracellular vesicles are potentially great candidates for early cancer detection because their contents have useful information to represent the status of their parental cells. Previous studies have revealed that different diseases including cancer have an association with the quantity of EVs and contents[88], [89]. Therefore, monitoring the secretion and release of exosomes is crucial for the early diagnosis of cancer.

Size quantification of small vesicles is essential for discriminating them based on their parental cells. Furthermore, studying the relationship between EV numbers in body fluids and disease is critical for biomarker discovery. However, the quantification of EVs such as exosomes is challenging because of their size. Hence, various methods of quantifying EVs have emerged. TRPS is one of the evolving techniques to quantify EVs of various sizes. TRPS technology has the potential to quantify small ionic resistive pulse currents to determine EV size, concentration, and zeta potential in one device but there are practical challenges related to the quantification in the lower size range. This limitation in sensitivity may justify the cause for variability in the quantification results of EVs[90]. The improvement of temporal resolution is closely related to the method of reducing noise. Strategies capable of reducing the magnitude of noise facilitate the quantification of smaller nanoscale EV populations[91]. Improving the size range limitations and sensitivity in TRPS requires introducing new device designs.

The development of new electronic devices for different advanced engineering applications requires innovations in the design of shielded enclosures to reduce electromagnetic interference[92]. There have been several investigations on newly proposed composite materials for electromagnetic shielding. The idea of choosing a composite material for a new shield design is to combine two or more different materials to improve shielding effectiveness Cezar et al. compared the shielding performance of composite materials with metal and investigated that composite materials are more efficient. Magnetic materials are applicable to shield low-frequency magnetic fields whereas good conductors are suitable to shield electric fields and high-frequency magnetic fields. Over the past two decades, acoustic metamaterials have been studied for low-frequency noise attenuation, and polyurethane is one of them with good sound-absorbing properties[93]. Combining materials with different electrical and mechanical

properties improves shielding effectiveness. A shielded enclosure that combines a metal covered with an insulator provides the largest reflection for the striking electric field. A shielding material with shielding effectiveness (SE) of less than 10 dB is considered a poor shield.

In this investigation, to improve the lower detection limit of tunable resistive pore sensors, an aluminum-coated metamaterial shield enclosure was designed to mitigate external noise. Using simulation as a guide, three different shield enclosure models were proposed to reduce external noise. A spectrum analyzer was used to analyze electromagnetic interference inside and outside the shielding cage. Moreover, to evaluate the effect of shielding on the TRPS system for the lower detection limit, size quantification of EVs was performed under shielded and unshielded conditions.

3. MATERIALS AND METHODS

3.1. Simulation and assembly of the shield enclosure

Previous studies have shown that the trans-membrane noise current in TRPS measurements appears to follow a Gaussian distribution[78]. For this Gaussian noise, a flow simulation computational fluid dynamics package was used to simulate the shielding effect of the polyurethane foam acoustic metamaterial. The simulation was performed using SolidWorks 2020 software, which has a plugin to perform flow simulation for broadband noise prediction. Three different panel structure designs were proposed for sound absorption capability and acoustical performances to reduce acoustic noise. The designed acoustic metasurface consists of an array of multiple absorption unit cells. In the simulation, 30-unit cells were selected to evaluate the acoustic power level of polyurethane metasurface under the shielded condition. The unshielded condition was simulated by removing the front panel.

Electromagnetic interference and mechanical vibrations are external noise sources that affect electrical measurements. The acoustic insulation was the strategy chosen to reduce noise arising from vibration. To reduce low-frequency acoustic noise in this study, three different foam resonator facade design patterns, for the metasurface of the shielded enclosure, were proposed. Of the three different proposed acoustic foam resonator structures models, model two was chosen based on simulation results. The selected shielded cage was built to reduce external noise using furring stripboard, acoustic foam soundproofing, tempered hardboard, and black foam boards. Also, an aluminum sheet was used to laminate the internal structure of the shield to replicate a Faraday cage that can reduce electromagnetic interference.

3.2. Electromagnetic and acoustic noise evaluation

To evaluate electromagnetic interference, Agilent technologies E4407B ESA- E series spectrum analyzer was used to measure power spectral density (PSD) within the shielded and unshielded conditions. Electrical and magnetic probes were connected to the spectrum analyzer in the PSD measurement, and measurement data was recorded. A noise level meter that could display noise data was used to record acoustic noise. The input transducer in the microphone converted environmental noise data to an electrical signal. After recording the noise data, MATLAB was used to obtain amplitude impulse response over time and spectrum level over frequency.

3.3. Preparation of polystyrene nanoparticles suspension

Colloid particle suspension was prepared using polystyrene beads that have a mean diameter of 210 nm. The stock concentration of polystyrene beads consisted of 7.3×10^{11} particles/mL. The stock solution was diluted to a dilution factor of 250 using a measuring electrolyte. The measuring electrolyte was prepared using 15 mL PBS and a 45 µL wetting solution (Izon Science).

3.4. Cell culture, extracellular vesicle collection, and sample preparation

Malignant cells were seeded at a density of 4×10^4 cells/mL onto 100 mm tissue culture plates[94], [95].[95] These plates contained 10 mL high glucose DMEM medium supplemented with 10% FBS. The plates were incubated at 37°C under 5% CO_2 for 48 hours or until the cells reached 80% confluency. When the cells reached 80% confluency, culture media was discarded, and the cells were washed twice with PBS. 10 mL of DMEM medium containing 10% exosomes depleted FBS was added to the plates. The plates were incubated at 37°C under 5% CO_2 for 48 hours. After the incubation period, the culture medium was collected and filtered through a 0.22

µm filter. Then, the filtered culture medium was centrifuged at 10,000g for 30 min to remove dead cells and large apoptotic debris. Following filtration, the culture medium was ultracentrifugation at 100,000 rpm for 70 minutes to remove larger vesicles and debris. The EVs were collected by discarding the supernatant and resuspending the pellet in 100 µL PBS.

3.5. TRPS instrument setup

The TRPS device (qNano, Izon sciences) was connected to the computer that has been installed with analysis software (Control Suite V3.4) via a USB port. The control suite software allows users to adjust different voltage settings to get optimal baseline current. The signal trace window displayed the magnitude of baseline and noise current.
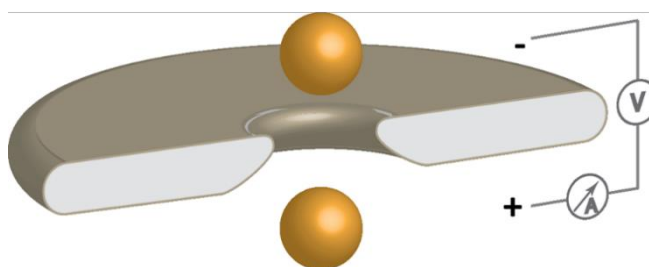

Figure 1. Schematic diagram of the TRPS nanopore setup.

The nanopore and the upper fluid cell were washed with deionized water, and the lower fluid cell was wetted with a measuring electrolyte followed by quickly removing the electrolyte. The nanopore was then mounted on the device and stretched to the experimental conditions. To establish a baseline current, a solution of 70 µL PBS was dispensed carefully in the lower fluid cell without introducing air bubbles that could cause a spike in noise current. Subsequently, 30 µL of PBS was added carefully into the upper fluid cell without introducing air bubbles. The solution in the upper fluid cell was adjusted by repetitive pipetting until a stable baseline current was established. Optimization of baseline current was done by selecting different DC bias voltages, stretching the nanopore at different lengths, and applying pressure at different ranges until the baseline current reached around 120 nA. The Polystyrene beads calibration particle was

then aspirated into the upper fluid cell to begin the translocation event. Translocation events of 500 calibration particles were tracked under the set conditions. After measurement, the upper fluid cell was washed with deionized water. Upon washing, 30 µL of EVs samples from malignant cells and nonmalignant cells were diluted appropriately using PBS and 0.05 % of Tween 20. Then a 30 µL sample was dispensed into the upper fluid cell to measure the magnitude of the blockade current. The blockade current was recorded by the control Suite V3.4 software for further analysis.

4. RESULTS AND DISCUSSION

4.1. Shielding effect on mechanical and electrical noise reduction

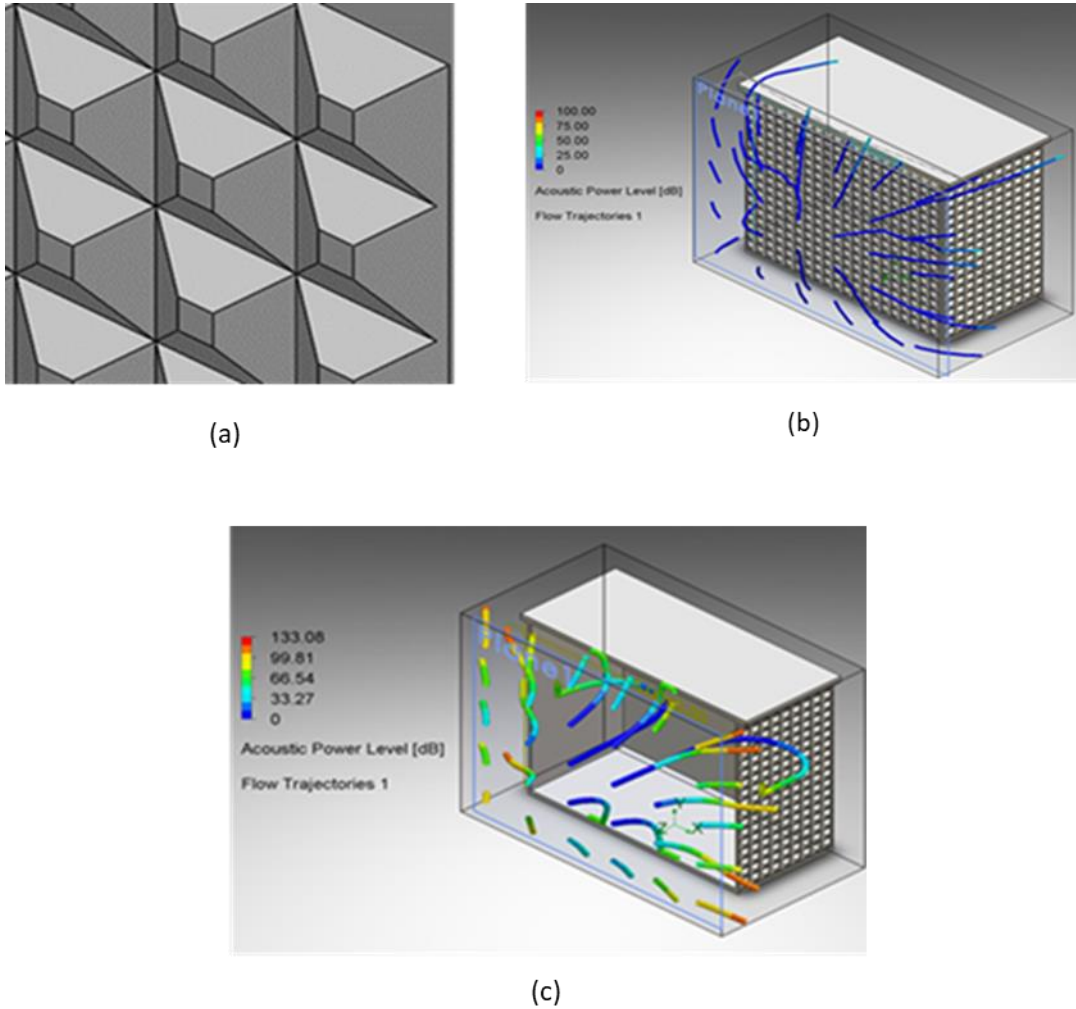### 4.1.1. Metacage design and simulation

(a)

(b)

(c)

Figure 2. Model 1 metacage design and acoustic power level (APL) simulation result. (a) Model 1 facade design pattern. (b) APL in shielded condition. (c) APL in unshielded condition.

Major noise sources of the TRPS system include external electrical sources, mechanical sources, and intrinsic noise of electronic circuits (Hz to MHz)[96]. The shielding performance of the acoustic metasurface was evaluated by selecting polyurethane conglomerate metamaterial from the flow simulation package. The three differing facade design patterns were compared to

the unshielded control and simulated to show deviation (Figures 2,4 and 5). The acoustic power

levels (APL) were calculated to predict noise as shown in Table 1. The difference in APL

between the shielded and unshielded conditions was used to predict shielding performance.

According to the simulation result, the average APL achieved a 70 dB difference for model one

design, 71 dB difference in the second model, and 65 dB difference in the third model. All three

models revealed the shielding performance of the metastructure in reducing acoustic noise.

Table 1. Simulation result of acoustic power levels.

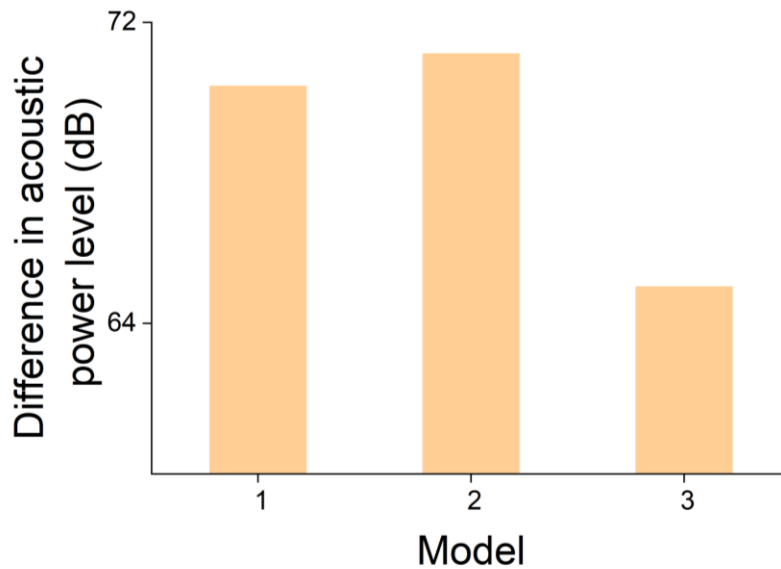| Model	APL (unshielded) dB	APL (shielded) dB	Difference between unshielded and shielded dB
Model 1	74.034	3.735	70
Model 2	77.289	6.135	71
Model 3	67.078	2.112	65

Figure 3. The differences in APL for the three models between shielded and unshielded
conditions.

As shown in Figure 3, the model two acoustic foam pattern showed more difference in

acoustic power level compared to the difference obtained in the other two proposed models, thus

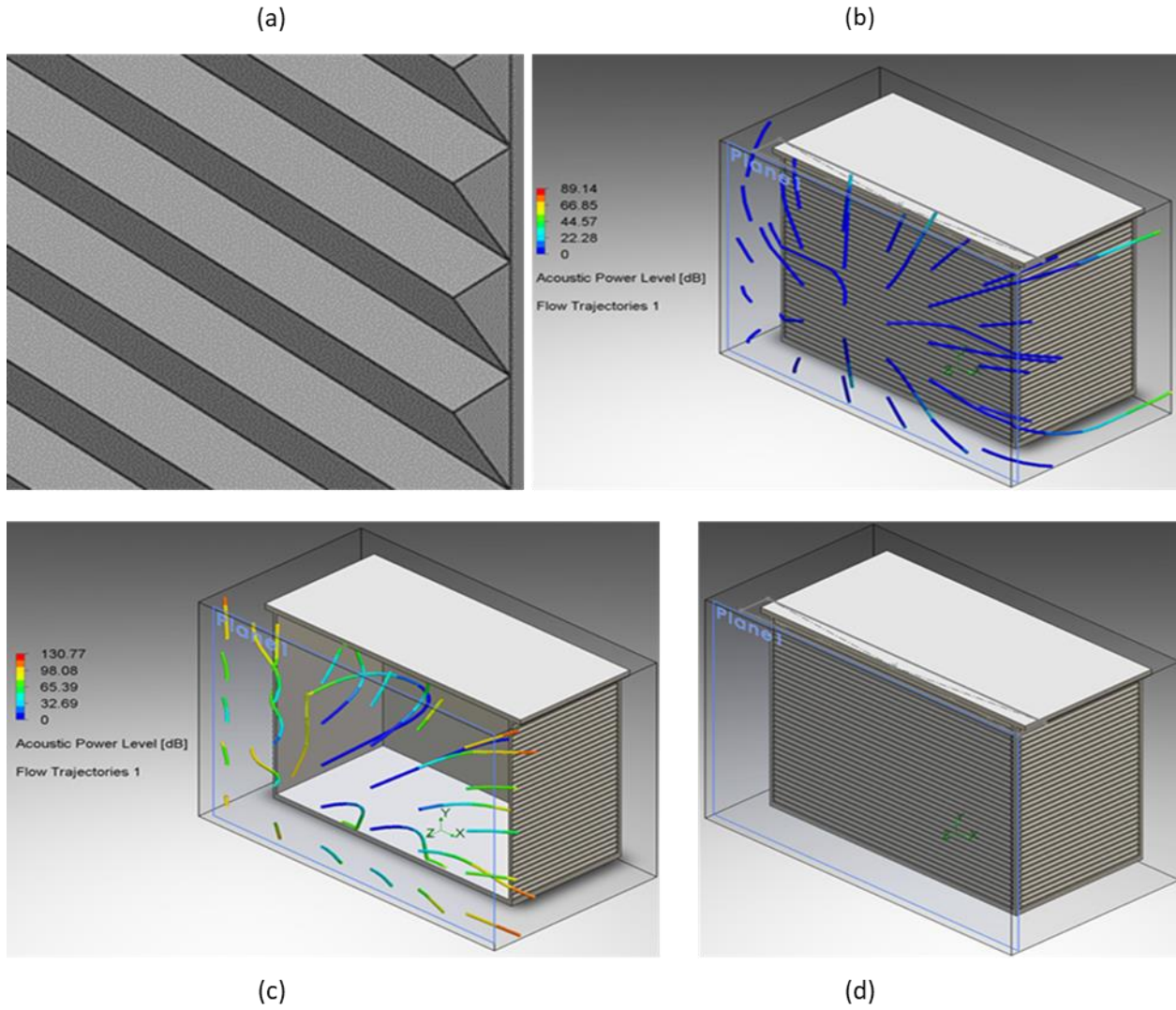model 2 was selected for assembly.

Figure 4. Model 2 metacage design and acoustic power level (APL) simulation result. (a) Model 2 facade design pattern. (b) APL in shielded condition. (c) APL in unshielded condition. (d) 3D design of model 2 shield enclosure.
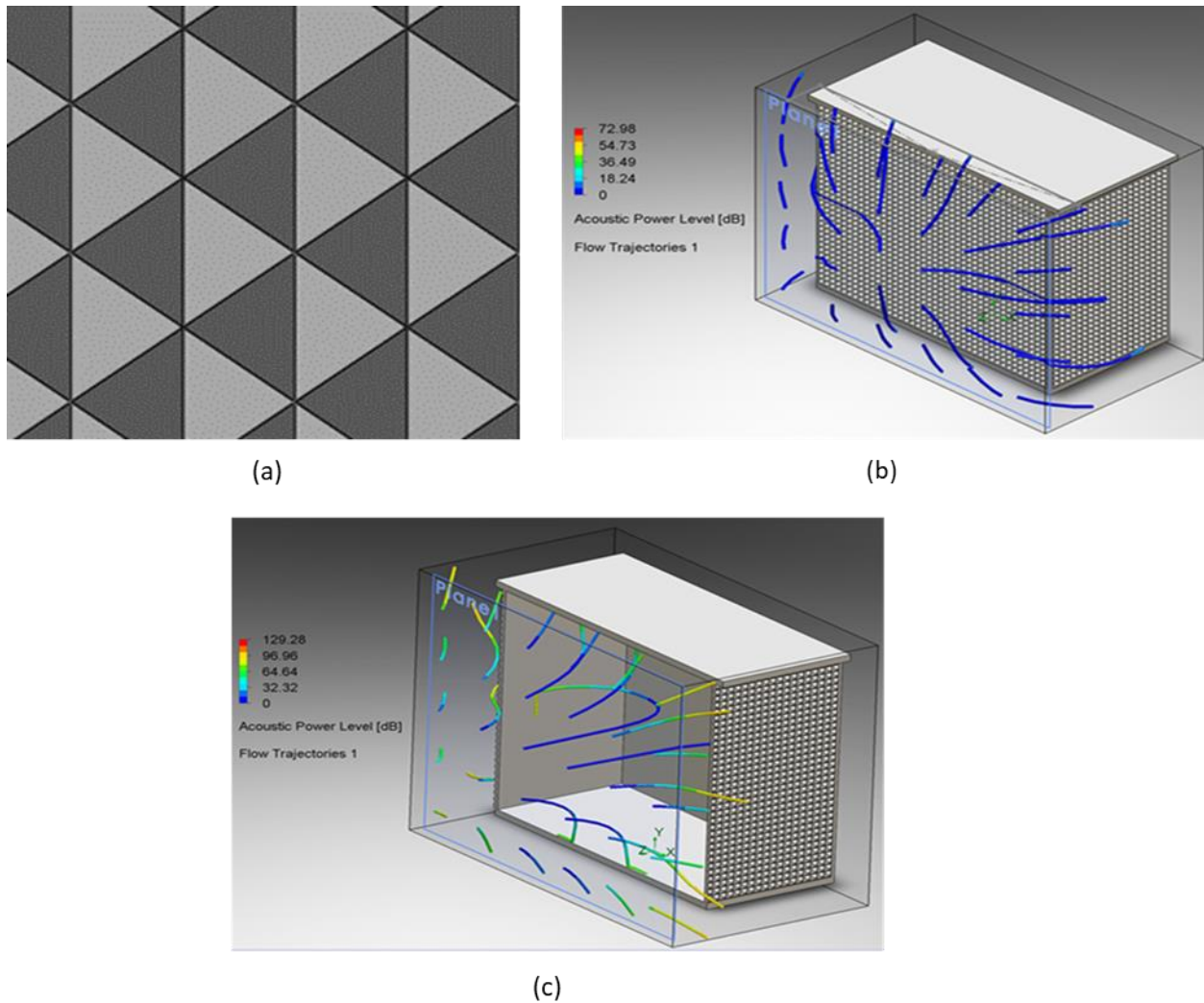
Figure 5. Model 3 metacage design and acoustic power level (APL) simulation result. (a) Model 2 facade design pattern. (b) APL in shielded condition. (c) APL in unshielded condition.

4.1.2. Shielding performance of acoustic metacage for low-frequency noise

Numerical simulation is crucial for accurate nanoparticle analysis to understand factors that influence the current response during translocation events, such as nanoparticle analyte surface charge, non-uniform electric fields, and forces on individual particles. The ability to obtain accurate nanoparticle characterization is crucial in applications such as the analysis of viruses and nanoparticles. To simulate this complex physics of translocation events, different models have been reported in published studies, including the Multiple Ion Model (MIM) using

finite element simulations. In this study, the use of flow simulation scope is to evaluate the

shielding performance of acoustic metamaterial to mitigate external noise interference during

TRPS measurement. Among the three abovementioned design models, model two (Figure 4d),

with the highest sound insulation performance in the simulation, was used to build the wrapper

enclosure. The noise reduction performance of the shielding enclosure was tested. The

logarithmic measurement of sound level relative to a reference noise was recorded in shielded

and unshielded conditions. The data in the time domain (Figure 6) and the spectral analysis result

(Figure 7) were plotted.
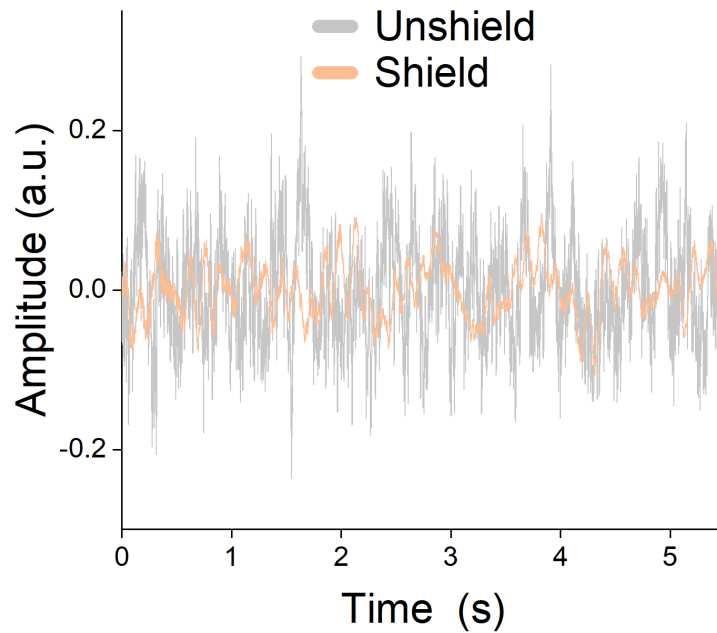
Figure 6. Time-domain representation of measured sound signals under the shielded and
unshielded conditions.

The sampled time-domain sound levels under the shielded and unshielded conditions

were compared in Figure 6. The sound levels measured inside the shielded enclosure showed a

reduction compared to the unshielded condition. Frequency response analysis was conducted,

and the spectrum periodograms were given in Figure 7. Reduced spectrum levels were observed

when comparing the shielded enclosure to the unshielded condition. Particularly, at the low-frequency range, 0-6.6 kHz, the spectrum level of the shielded condition was significantly lower than the unshielded condition, while the spectrum level difference at other frequency ranges was noticeably constant. This suggests that the enclosure selectively filtered low-frequency acoustic noise.
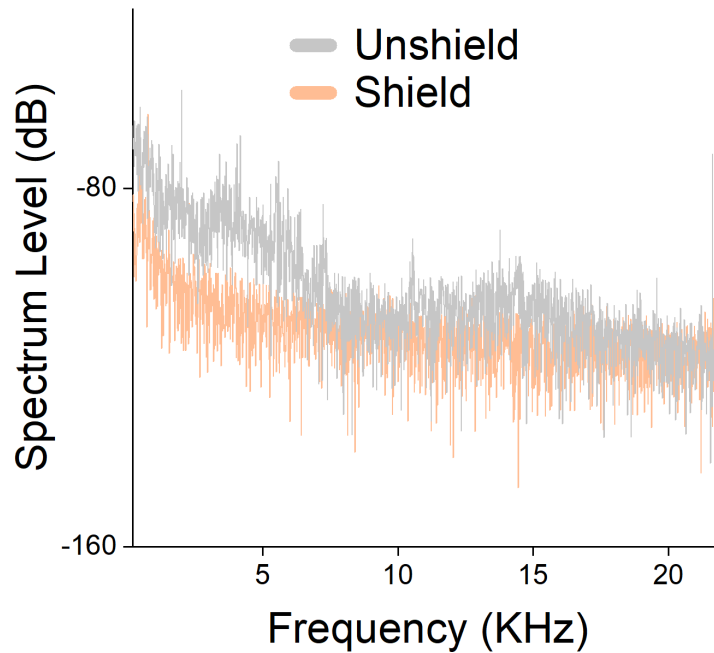
Figure 7. Frequency response of measured sound signals under the shielded and unshielded conditions.

To confirm the reproducibility of the soundproof effect, 50 random recordings (5s each, Figure 8a) were analyzed for root mean square (RMS) noise level. The minimum, maximum, and average of the 50 RMS values suggested that the shielded condition had lower RMS noise levels (Figure 8b). The mean value of RMS noise inside the shielded enclosure shows a reduction compared to the unshielded condition (3.236 vs 4.886 dB), which is statistically significant by t-test (Figure 8c). These results validated the shielding performance of the acoustic metamaterial as expected in the simulation.

Figure 8. RMS noise measurements of low-frequency noise.
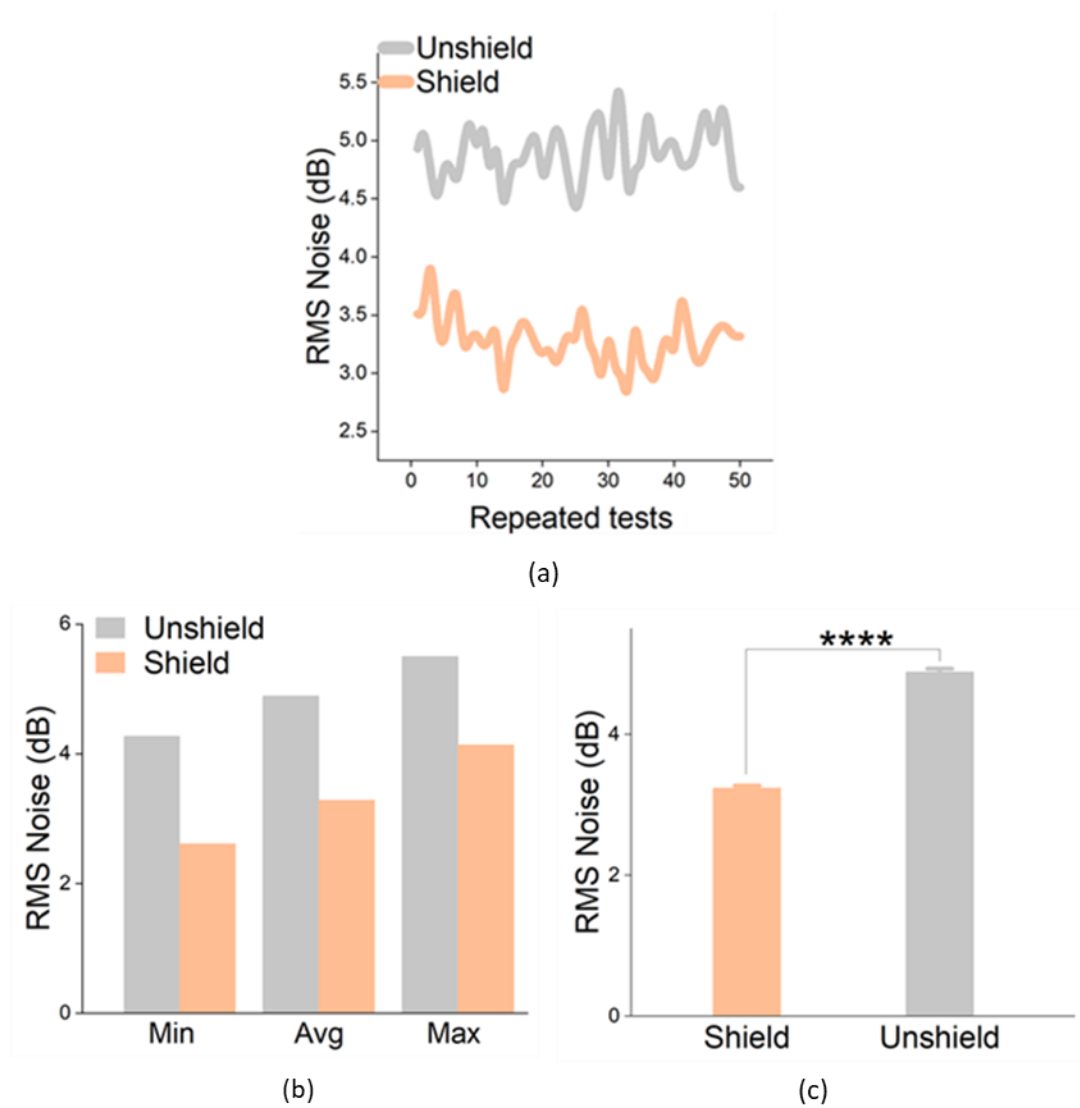(a) RMS noise (dB) of 50 repeated measurements. (b) Comparison of the min, average, and maximum value of measured RMS noise. (c) The statistical test result of RMS noise level under shielded and unshielded conditions. ****$P < 0.0001$. a.u.: arbitrary units.

4.1.3. Shielding effectiveness test for external electromagnetic interference
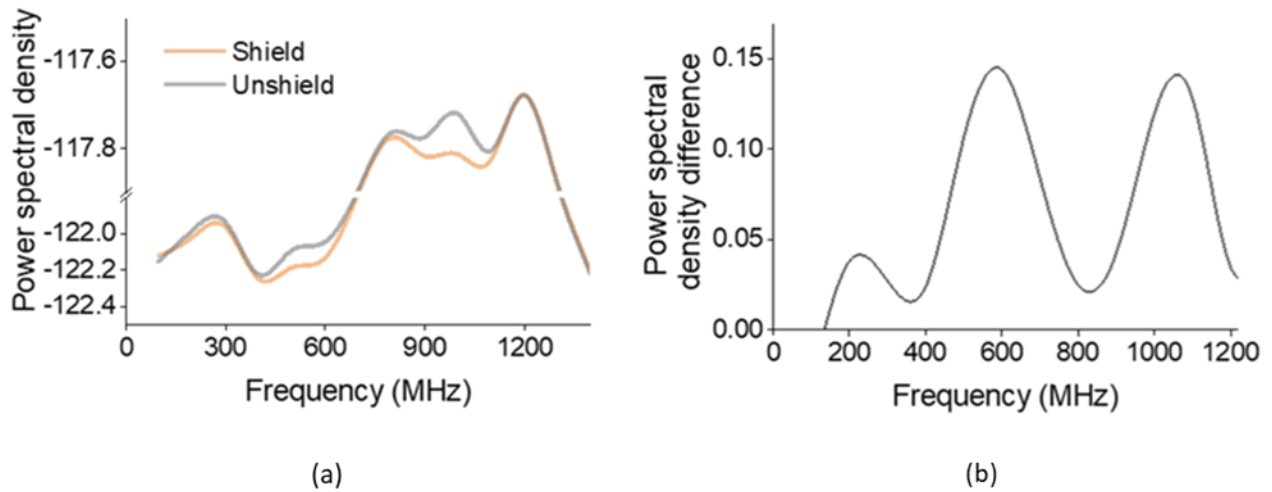

Figure 9. Electromagnetic interference test result.
(a) Power spectral density of noise within and outside the shielded enclosure. (b) The change in power spectral density between the shielded and unshielded conditions.

The external electromagnetic field can directly interact with ions in the electrolyte during translocation events, thus affecting the TRPS measurements. When the RMS noise level exceeds 20 nA, the possible cause is due to electrical interference[97]. To reduce interference of external electromagnetic fields, the enclosure was laminated with a grounded conductive aluminum sheet inside. A spectrum analyzer was used to investigate electromagnetic noise inside and outside the shielding environment. Lower power spectral density was observed under the shielded condition over the tested frequency (Figure 9a). The power spectral density difference between the shielded and unshielded conditions varied with the frequency range (Figure 9b). The two frequency ranges, 400-600 MHz and 900-1200 MHz showed significant differences. Wireless telecommunication carriers operate near these two frequency ranges. Therefore, the shielding cage can be used to reduce external noise coming from a device working at 600 MHz and 900 MHz (GSM) frequency ranges.

4.2. Shielding effect on resistive pulse current sensing of nanoparticles

4.2.1. Shielding effect on the quantification of polystyrene nanoparticles

The shielding effect on the TRPS quantification method was first evaluated by testing standard nanoparticles, known as polystyrene beads, commonly used as a quantification and characterization reference[98]. The RMS value of translocation current (nA) was then recorded for noise assessment. In Figure 10a, the RMS noise was significantly reduced (> 30 %) with the shielding when using TRPS to quantify polystyrene nanoparticles. The impact of the noise reduction on the quantification was analyzed through the size profiling of the standard polystyrene beads with a mean diameter of 210 nm. The beads were quantified using TRPS with and without the shielding. The size distribution curve exhibited a downward (left) shift from unshielded to the shielded condition (Figure 10b). The center of distribution under the shielded condition was proximate to the actual diameter of the standard polystyrene beads used for the test, suggesting the shield ensured precise quantification. Together with the abovementioned noise reduction result (mechanical and electromagnetic), the reduction of low-level noise current led to better quantification performance for lower-sized nanoparticles, which affirmed the benefit of using the shielded enclosure for small resistive pulse current sensing of nanoparticles.

In resistive pulse current sensing of nanoparticles, a bias voltage establishes current due to electrophoresis. Then particles pass through a nanopore under the influence of electrokinetic forces. Gaurav et al. [99] demonstrated the higher potential due to the applied positive voltage results in a larger ratio of the change in ionic current to the baseline current, while the applied negative bias results in a smaller value of the resistive pulse signal to the baseline current. In this study, the same DC bias voltage was maintained during resistive pulse sensing in a shielded and unshielded environment, to evaluate the impact of external EMI on electrical measurements.
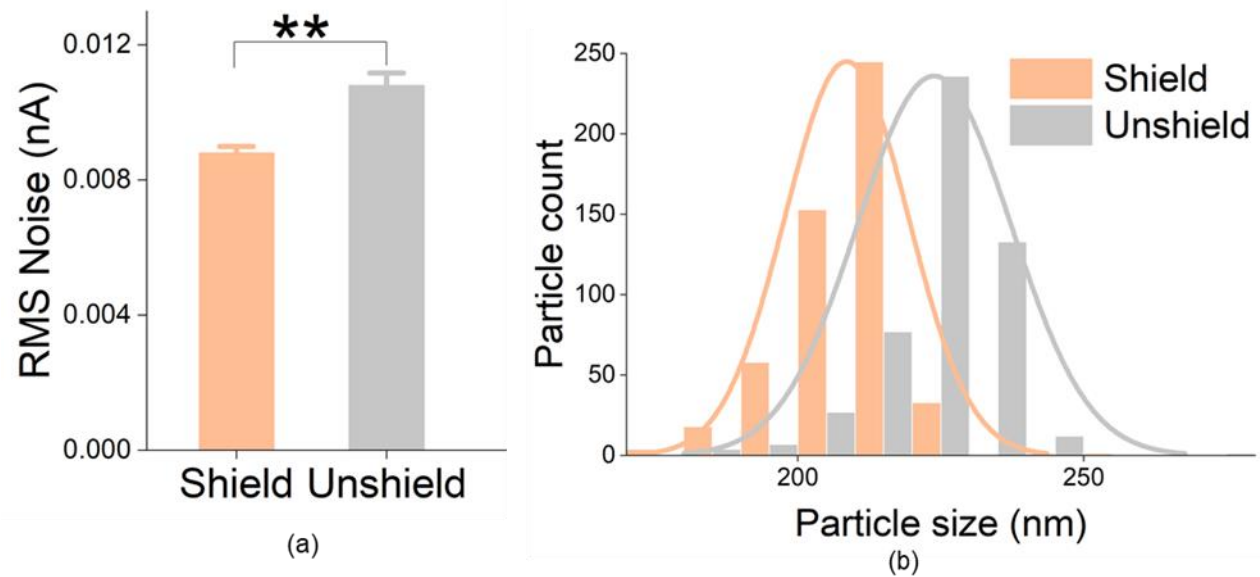
Figure 10. Shielding effect on the noise reduction and quantification of polystyrene nanoparticles.
(a) RMS noise of TRPS measurement inside and outside the shielded enclosure. (b) Size distribution of polystyrene beads when quantification was performed inside and outside the shielded enclosure. Data points represent mean ± SE (n=5). **$P < 0.01$.

4.2.2. Shielding effect on EVs quantification

To evaluate the impact of shielding on the quantification of bio-originated particles, EVs from malignant (Mia PaCa-2) and nonmalignant (HPNE) cells were profiled using TRPS with and without the shielding. Similar to the polystyrene beads (Figure 10a), the RMS noise was significantly reduced with the shielding cage when using TRPS (Figures 11a and b). However, the RMS change from shield to the unshielded condition of the nonmalignant EVs is dramatic (>30 %).
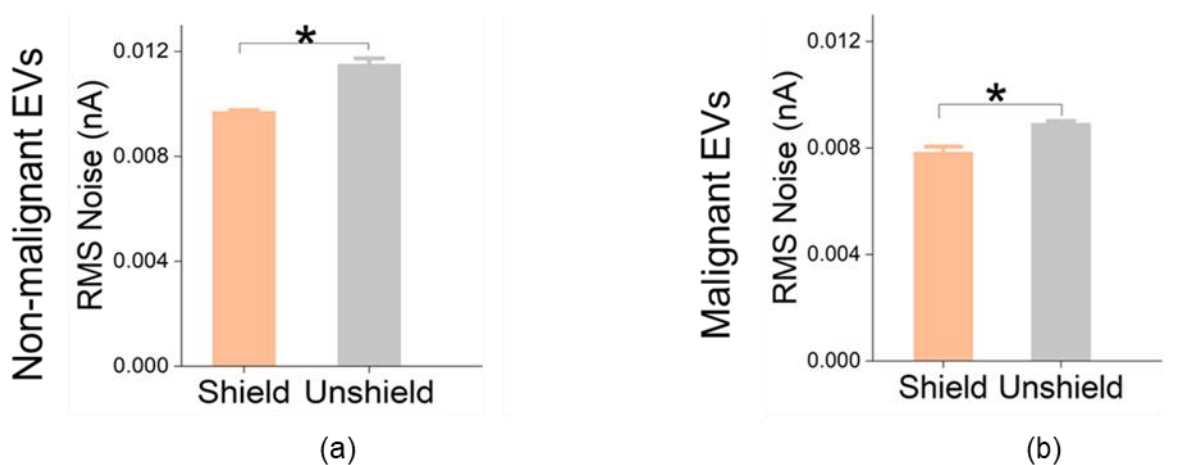
Figure 11. RMS noise measurements during resistive pulse sensing of EVs.
Data points represent mean ± SE (n=4). *$P < 0.05$.

Correspondingly, the size distribution curve exhibited a downward (left) shift from

unshielded to the shielded condition (Figures 12a and b). However, consistent with the RMS

change, the distribution shift of nonmalignant EVs is more observable. When quantifying EVs

inside the shielded enclosure, the noise was reduced which enhanced the minimum size detection

limit.
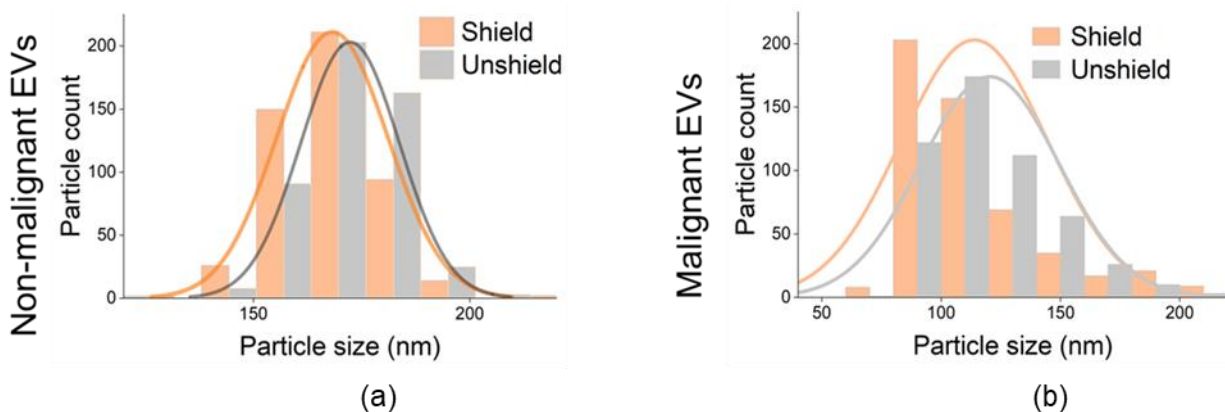
Figure 12. Size distribution of nonmalignant and malignant EVs.
(a) Size distribution of EVs from nonmalignant cells inside and outside the shielded enclosure.
(b) Size distribution of EVs from malignant cells inside and outside the shielded enclosure.

The advanced detection limit of nanosized particles, therefore, enabled a broader size

range of the TRPS profiling. This has increased the precision of nanoparticles quantification, and

thus empowers a more accurate size comparison of EVs from malignant cells and nonmalignant

cells. The advanced size profiling facilitates the diagnostic application of TRPS in discriminating

tumor-derived EVs from other EVs (Figures 13a and b).
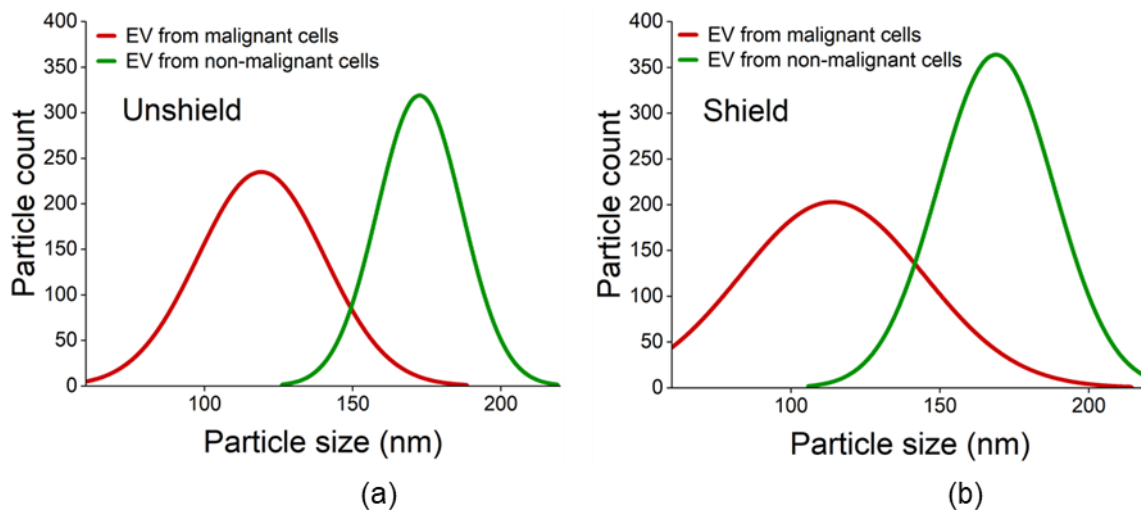
Figure 13. Size distribution of EVs collected from the malignant and nonmalignant cells with
and without the shielded enclosure.
(a) Size distribution of EVs from malignant and nonmalignant cells quantified under the
unshielded enclosure. (b) Size distribution profile of EVs from malignant and nonmalignant cells
quantified under the shielded enclosure.

4.2.3. Shielding effect on particle translocation events arrival time

In resistive pulse current sensing, when a target analyte passes through a pore with an

electric field, it results in a dip in ionic current. Such changes in the ionic current manifest as

resistive pulses and these events are called translocation events. Size profiling using qNANO

TRPS requires at least 500 translocation events to obtain a statistically meaningful size

evaluation. A resistive pulse signal can be covered by noise when the resistive pulse magnitude

of a small particle is less than the magnitude of noise. To observe blockade events in the TRPS

system, a noise level of less than 10 pA is required[100]. The designed shield enclosure reduced

environmental noise and in turn enabled the detection of smaller nanosized signals (nA) that

were covered due to the high magnitude of noise current. This led to a longer recording time to

reach the minimum statistical count. The recording time was compared with and without the

shield using polystyrene beads and EVs (Figures 14 and 15). All shield conditions manifested

longer elapsed time, which is consistent with the aforementioned.
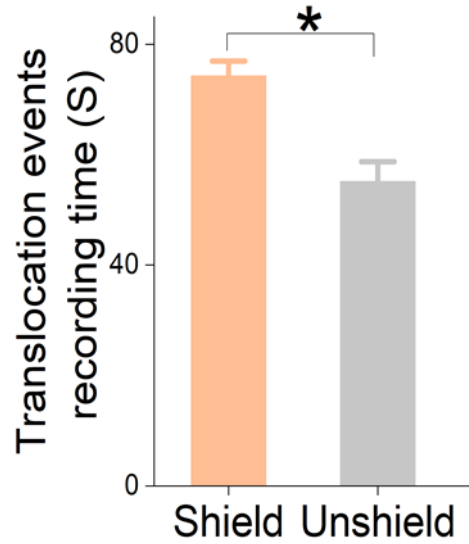
Figure 14. The time required to record the current trace of polystyrene particles translocation
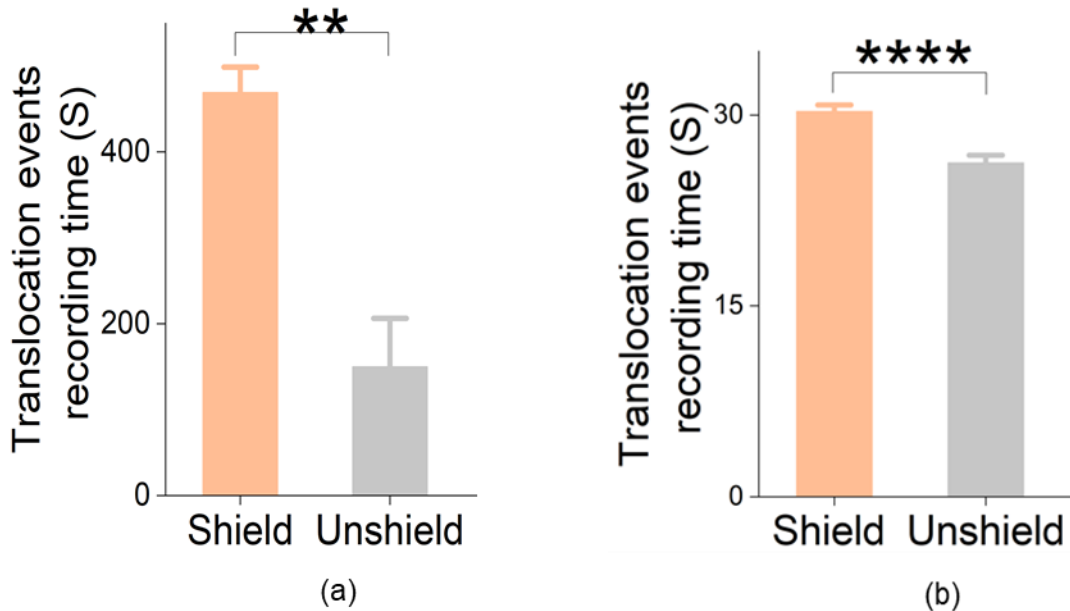events

Figure 15. Elapsed time to record current traces during translocation events of EVs
(a) Elapsed time to record current trace when nonmalignant EVs traversed through the nanopore.
(b) Elapsed time to record current trace when malignant EVs traversed through the nanopore.
Data points represent mean ± SE (n=4). *P < 0.05; **P < 0.01; ****P < 0.0001.

The electric field intensity is an important parameter for controlling the particle transport velocity and the current fluctuation amplitude. To accurately profile the particle size, the particle is required to pass through the Z-axis (centerline) of the pore. Off-axial particle translocation events are phenomena in which particles do not pass through the center of a pore and result in a higher-than-expected resistive pulse size. This issue affects measurement sensitivity and detection range. Reducing the influence of unwanted fluctuating external electric field noise in the vicinity of the nanopore device facilitates particle translocation to the center of the pore's axial axis. Enclosing the resistive pulse sensing device with the shielded cage reduces the coupling of external electric field noise to the non-uniform electric field established due to electrophoresis. Previous studies by Lener et al. [88] have introduced hydrodynamic focusing to keep the particle path at the centerline of the microfluidic channel in microfluidic resistive pulse sensing. However, the assumption that translocation events occur only in the pore center may also lead to underestimation in determining particle size. Choi et al. [101] demonstrated the variation in the arrival time of translocation events from channel to channel in microfluidic resistive pulse sensing. This suggests that particles prefer specific channels for translocation events.

The resolution of the nanopore sensor could also be enhanced either by retarding the particle translocation or by increasing the data acquisition frequency of the measurement system. Conventional Bessel filters for data acquisition in TRPS fail to track short-lived translocation events[102]. Furthermore, most existing nanopore sensors use a single channel to track translocation data. The ability to record fast translocation data enables high data throughput. However, tracking undetectable short-lived translocation events requires a novel filter design for resistive pulse sensors to reduce electrical noise. In addition, ion concentration and applied DC

bias voltage can affect particle translocation events[103]. Moreover, translocation events per minute decrease when the analyte concentration increases. In this study, the same concentration was maintained when quantification was performed with and without the shielded cage, and all other conditions were set identical, thus ruling out the impact of parameters other than the noise. Also, in 2013, Goyal et al. [104] published a paper in which they described that electrokinetic forces acting on nanoparticles require additional force such as applied pressure to analyze high particle motion in very short-range nanopore sensors. Such pressures can be used to counterbalance electrokinetic forces in TRPS measurements. This optimization helps to slow down the velocity of nanoparticles and allows to record more translocation events for a longer time. The ability to record more translocation events over longer periods improves the lower limit of detection. In this research, the same pressure was maintained under shielded and unshielded conditions to investigate the effect of shielding in detecting smaller resistive pulse signals.

A previous study has shown that in physiological salt environments, individual particles can diffuse through nanopores without an electric field, a phenomenon known as a diffusion event[99]. Diffusion events allow the characterization of biological nanoparticles independent of the electrodynamic forces generated by the electric field. Electrokinetic-independent particle motion facilitates the characterization of biological nanoparticles in their native state.

5. CONCLUSION

Maintaining a noise-free setup is essential for elaborated analysis equipment. However, inevitable environmental noise is a common challenge deteriorating the sensitivity of resistive pulse current sensing. In this study, a shielded enclosure was designed to reduce the impact of environmental noise (mechanical and electromagnetic) on the TRPS measurement. The acoustic insulation function of the enclosure was achieved using a patterned façade design metasurface which has been optimized by simulation. Electromagnetic noise interference was weakened by coating grounded conductive aluminum sheets inside the enclosure. As a result, the external noise was significantly reduced, and the signal-to-noise ratio was improved when using the shielded enclosure. The precision improvement was validated by using standard polystyrene nanoparticles. To validate the advanced detection limit on bio-originated particles, EVs from malignant cells and nonmalignant cells were profiled using TRPS with and without the shielding enclosure. Shielding significantly reduced the noise and improved the lower detection limit of TRPS. This enhances a more accurate comparison of the size of EVs derived from malignant and nonmalignant cells. The shield design facilitates the search for a sensitive analytical system to quantify small EVs and improves the sensitivity of the TRPS.

REFERENCES

[1]   E. van der Pol, A. N. Böing, E. L. Gool, and R. Nieuwland, "Recent developments in the nomenclature, presence, isolation, detection and clinical impact of extracellular vesicles," *Journal of Thrombosis and Haemostasis*, vol. 14, no. 1, pp. 48–56, Jan. 2016, doi: 10.1111/jth.13190.

[2]   G. R. Dubyak, "P2X7 receptor regulation of non-classical secretion from immune effector cells," *Cellular Microbiology*, vol. 14, no. 11, pp. 1697–1706, Nov. 2012, doi: 10.1111/cmi.12001.

[3]   N. M. McKechnie, B. C. R. King, E. Fletcher, and G. Braun, "Fas-ligand is stored in secretory lysosomes of ocular barrier epithelia and released with microvesicles," *Experimental Eye Research*, vol. 83, no. 2, pp. 304–314, Aug. 2006, doi: 10.1016/j.exer.2005.11.028.

[4]   D. Virgintino *et al.*, "Plasma membrane-derived microvesicles released from tip endothelial cells during vascular sprouting," *Angiogenesis*, vol. 15, no. 4, pp. 761–769, Dec. 2012, doi: 10.1007/s10456-012-9292-y.

[5]   A. C. Matzdorff, D. Berchner, G. Kühnel, B. Kemkes-Matthes, H. Pralle, and R. Voss, "Relative and Absolute Changes of Activated Platelets, Microparticles and Platelet Aggregates after Activation in vitro," *Pathophysiology of Haemostasis and Thrombosis*, vol. 28, no. 6, pp. 277–288, 1998, doi: 10.1159/000022444.

[6]   M. Baj-Krzyworzeka, R. Szatanek, K. Węglarczyk, J. Baran, and M. Zembala, "Tumour-derived microvesicles modulate biological activity of human monocytes," *Immunology Letters*, vol. 113, no. 2, pp. 76–82, Nov. 2007, doi: 10.1016/j.imlet.2007.07.014.

[7]   V. Luga *et al.*, "Exosomes Mediate Stromal Mobilization of Autocrine Wnt-PCP Signaling in Breast Cancer Cell Migration," *Cell*, vol. 151, no. 7, pp. 1542–1556, Dec. 2012, doi: 10.1016/j.cell.2012.11.024.

[8]   H. Peinado *et al.*, "Melanoma exosomes educate bone marrow progenitor cells toward a pro-metastatic phenotype through MET," *Nature Medicine*, vol. 18, no. 6, pp. 883–891, Jun. 2012, doi: 10.1038/nm.2753.

[9]   M. Yáñez-Mó *et al.*, "Biological properties of extracellular vesicles and their physiological functions," *Journal of Extracellular Vesicles*, vol. 4, no. 1, p. 27066, Jan. 2015, doi: 10.3402/jev.v4.27066.

[10]   C. Bang and T. Thum, "Exosomes: New players in cell–cell communication," *The International Journal of Biochemistry & Cell Biology*, vol. 44, no. 11, pp. 2060–2064, Nov. 2012, doi: 10.1016/j.biocel.2012.08.007.

[11]   L. Urbanelli *et al.*, "Signaling Pathways in Exosomes Biogenesis, Secretion and Fate," *Genes*, vol. 4, no. 2, pp. 152–170, Mar. 2013, doi: 10.3390/genes4020152.

[12]   G. Midekessa *et al.*, "Zeta Potential of Extracellular Vesicles: Toward Understanding the Attributes that Determine Colloidal Stability," *ACS Omega*, vol. 5, no. 27, pp. 16701–16710, Jul. 2020, doi: 10.1021/acsomega.0c01582.

[13]   G. Müller, "Microvesicles/exosomes as potential novel biomarkers of metabolic diseases," *Diabetes, Metabolic Syndrome and Obesity: Targets and Therapy*, p. 247, Aug. 2012, doi: 10.2147/DMSO.S32923.

[14]   B. Vestad *et al.*, "Size and concentration analyses of extracellular vesicles by nanoparticle tracking analysis: a variation study," *Journal of Extracellular Vesicles*, vol. 6, no. 1, p. 1344087, Dec. 2017, doi: 10.1080/20013078.2017.1344087.

[15]   F. Momen-Heravi *et al.*, "Current methods for the isolation of extracellular vesicles," *Biological Chemistry*, vol. 394, no. 10, pp. 1253–1262, Oct. 2013, doi: 10.1515/hsz-2013-0141.

[16]   K. Boriachek *et al.*, "Biological Functions and Current Advances in Isolation and Detection Strategies for Exosome Nanovesicles," *Small*, vol. 14, no. 6, p. 1702153, Feb. 2018, doi: 10.1002/smll.201702153.

[17]   I. Helwa *et al.*, "A Comparative Study of Serum Exosome Isolation Using Differential Ultracentrifugation and Three Commercial Reagents," *PLOS ONE*, vol. 12, no. 1, p. e0170628, Jan. 2017, doi: 10.1371/journal.pone.0170628.

[18]   E. van der Pol, A. N. Böing, P. Harrison, A. Sturk, and R. Nieuwland, "Classification, Functions, and Clinical Relevance of Extracellular Vesicles," *Pharmacological Reviews*, vol. 64, no. 3, pp. 676–705, Jul. 2012, doi: 10.1124/pr.112.005983.

[19]   C. Rajagopal and K. B. Harikumar, "The Origin and Functions of Exosomes in Cancer," *Frontiers in Oncology*, vol. 8, Mar. 2018, doi: 10.3389/fonc.2018.00066.

[20]   N. Coltel, V. Combes, S. C. Wassmer, G. Chimini, and G. E. Grau, "Cell vesiculation and immunopathology: implications in cerebral malaria," *Microbes and Infection*, vol. 8, no. 8, pp. 2305–2316, Jul. 2006, doi: 10.1016/j.micinf.2006.04.006.

[21]   L. Azevedo, M. Pedro, and F. Laurindo, "Circulating Microparticles as Therapeutic Targets in Cardiovascular Diseases," *Recent Patents on Cardiovascular Drug Discovery*, vol. 2, no. 1, pp. 41–51, Jan. 2007, doi: 10.2174/157489007779606121.

[22]   Y. Meng, S. Kang, and D. A. Fishman, "Lysophosphatidic acid stimulates fas ligand microvesicle release from ovarian cancer cells," *Cancer Immunology, Immunotherapy*, vol. 54, no. 8, pp. 807–814, Aug. 2005, doi: 10.1007/s00262-004-0642-5.

[23]   L. G. Lima, R. Chammas, R. Q. Monteiro, M. E. C. Moreira, and M. A. Barcinski, "Tumor-derived microvesicles modulate the establishment of metastatic melanoma in a phosphatidylserine-dependent manner," *Cancer Letters*, vol. 283, no. 2, pp. 168–175, Oct. 2009, doi: 10.1016/j.canlet.2009.03.041.

[24] L. Balaj *et al.*, "Tumour microvesicles contain retrotransposon elements and amplified oncogene sequences," *Nature Communications*, vol. 2, no. 1, p. 180, Sep. 2011, doi: 10.1038/ncomms1180.

[25] C. Grange *et al.*, "Microvesicles Released from Human Renal Cancer Stem Cells Stimulate Angiogenesis and Formation of Lung Premetastatic Niche," *Cancer Research*, vol. 71, no. 15, pp. 5346–5356, Aug. 2011, doi: 10.1158/0008-5472.CAN-11-0241.

[26] S. Wan, Z. Zhou, B. Duan, and L. Morel, "Direct B cell stimulation by dendritic cells in a mouse model of lupus," *Arthritis & Rheumatism*, vol. 58, no. 6, pp. 1741–1750, Jun. 2008, doi: 10.1002/art.23515.

[27] S. K. Gupta, C. Bang, and T. Thum, "Circulating MicroRNAs as Biomarkers and Potential Paracrine Mediators of Cardiovascular Disease," *Circulation: Cardiovascular Genetics*, vol. 3, no. 5, pp. 484–488, Oct. 2010, doi: 10.1161/CIRCGENETICS.110.958363.

[28] A. S. Azmi, B. Bao, and F. H. Sarkar, "Exosomes in cancer development, metastasis, and drug resistance: a comprehensive review," *Cancer and Metastasis Reviews*, vol. 32, no. 3–4, pp. 623–642, Dec. 2013, doi: 10.1007/s10555-013-9441-9.

[29] B. Costa-Silva *et al.*, "Pancreatic cancer exosomes initiate pre-metastatic niche formation in the liver," *Nature Cell Biology*, vol. 17, no. 6, pp. 816–826, Jun. 2015, doi: 10.1038/ncb3169.

[30] R. Vogel *et al.*, "A standardized method to determine the concentration of extracellular vesicles using tunable resistive pulse sensing," *Journal of Extracellular Vesicles*, vol. 5, no. 1, p. 31242, Jan. 2016, doi: 10.3402/jev.v5.31242.

[31] S. Gurung, D. Perocheau, L. Touramanidou, and J. Baruteau, "The exosome journey: from biogenesis to uptake and intracellular signalling," *Cell Communication and Signaling*, vol. 19, no. 1, p. 47, Dec. 2021, doi: 10.1186/s12964-021-00730-1.

[32] M. Logozzi *et al.*, "High Levels of Exosomes Expressing CD63 and Caveolin-1 in Plasma of Melanoma Patients," *PLoS ONE*, vol. 4, no. 4, p. e5219, Apr. 2009, doi: 10.1371/journal.pone.0005219.

[33] T. Pisitkun, R.-F. Shen, and M. A. Knepper, "Identification and proteomic profiling of exosomes in human urine," *Proceedings of the National Academy of Sciences*, vol. 101, no. 36, pp. 13368–13373, Sep. 2004, doi: 10.1073/pnas.0403453101.

[34] A. Michael *et al.*, "Exosomes from human saliva as a source of microRNA biomarkers," *Oral Diseases*, vol. 16, no. 1, pp. 34–38, Jan. 2010, doi: 10.1111/j.1601-0825.2009.01604.x.

[35] S. Keller *et al.*, "CD24 is a marker of exosomes secreted into urine and amniotic fluid," *Kidney International*, vol. 72, no. 9, pp. 1095–1102, Nov. 2007, doi: 10.1038/sj.ki.5002486.

[36]   F. Andre *et al.*, "Malignant effusions and immunogenic tumour-derived exosomes," *The Lancet*, vol. 360, no. 9329, pp. 295–305, Jul. 2002, doi: 10.1016/S0140-6736(02)09552-1.

[37]   D. Xiao *et al.*, "Identifying mRNA, MicroRNA and Protein Profiles of Melanoma Exosomes," *PLoS ONE*, vol. 7, no. 10, p. e46874, Oct. 2012, doi: 10.1371/journal.pone.0046874.

[38]   P. Ziaei, C. E. Berkman, and M. G. Norton, "Review: Isolation and Detection of Tumor-Derived Extracellular Vesicles," *ACS Applied Nano Materials*, vol. 1, no. 5, pp. 2004–2020, May 2018, doi: 10.1021/acsanm.8b00267.

[39]   R. M. Johnstone, M. Adam, J. R. Hammond, L. Orr, and C. Turbide, "Vesicle formation during reticulocyte maturation. Association of plasma membrane activities with released vesicles (exosomes).," *Journal of Biological Chemistry*, vol. 262, no. 19, pp. 9412–9420, Jul. 1987, doi: 10.1016/S0021-9258(18)48095-7.

[40]   K. Singh, R. Nalabotala, K. M. Koo, S. Bose, R. Nayak, and M. J. A. Shiddiky, "Separation of distinct exosome subpopulations: isolation and characterization approaches and their associated challenges," *The Analyst*, vol. 146, no. 12, pp. 3731–3749, 2021, doi: 10.1039/D1AN00024A.

[41]   R. T. Davies, J. Kim, S. C. Jang, E.-J. Choi, Y. S. Gho, and J. Park, "Microfluidic filtration system to isolate extracellular vesicles from blood," *Lab on a Chip*, vol. 12, no. 24, p. 5202, 2012, doi: 10.1039/c2lc41006k.

[42]   M. L. Merchant *et al.*, "Microfiltration isolation of human urinary exosomes for characterization by MS," *PROTEOMICS - Clinical Applications*, vol. 4, no. 1, pp. 84–96, Jan. 2010, doi: 10.1002/prca.200800093.

[43]   Z. Zhao, H. Wijerathne, A. K. Godwin, and S. A. Soper, "Isolation and analysis methods of extracellular vesicles (EVs)," *Extracellular Vesicles and Circulating Nucleic Acids*, 2021, doi: 10.20517/evcna.2021.07.

[44]   E. H. Koritzinsky, J. M. Street, R. A. Star, and P. S. T. Yuen, "Quantification of Exosomes," *Journal of Cellular Physiology*, vol. 232, no. 7, pp. 1587–1590, Jul. 2017, doi: 10.1002/jcp.25387.

[45]   J. Webber and A. Clayton, "How pure are your vesicles?," *Journal of Extracellular Vesicles*, vol. 2, no. 1, p. 19861, Jan. 2013, doi: 10.3402/jev.v2i0.19861.

[46]   R. Vogel *et al.*, "Quantitative Sizing of Nano/Microparticles with a Tunable Elastomeric Pore Sensor," *Analytical Chemistry*, vol. 83, no. 9, May 2011, doi: 10.1021/ac200195n.

[47]   C. Théry, M. Ostrowski, and E. Segura, "Membrane vesicles as conveyors of immune responses," *Nature Reviews Immunology*, vol. 9, no. 8, pp. 581–593, Aug. 2009, doi: 10.1038/nri2567.

[48] E. van der Pol, A. G. Hoekstra, A. Sturk, C. Otto, T. G. van Leeuwen, and R. Nieuwland, "Optical and non-optical methods for detection and characterization of microparticles and exosomes," *Journal of Thrombosis and Haemostasis*, vol. 8, no. 12, pp. 2596–2607, Dec. 2010, doi: 10.1111/j.1538-7836.2010.04074.x.

[49] J. P. Nolan and E. Duggan, "Analysis of Individual Extracellular Vesicles by Flow Cytometry," 2018, pp. 79–92. doi: 10.1007/978-1-4939-7346-0_5.

[50] X. Tan *et al.*, "Quantification and immunoprofiling of bladder cancer cell-derived extracellular vesicles with microfluidic chemiluminescent ELISA," *Biosensors and Bioelectronics: X*, vol. 8, p. 100066, Sep. 2021, doi: 10.1016/j.biosx.2021.100066.

[51] S.-C. Guo, S.-C. Tao, and H. Dawn, "Microfluidics-based on-a-chip systems for isolating and analysing extracellular vesicles," *Journal of Extracellular Vesicles*, vol. 7, no. 1, p. 1508271, Dec. 2018, doi: 10.1080/20013078.2018.1508271.

[52] W. Anderson, D. Kozak, V. A. Coleman, Å. K. Jämting, and M. Trau, "A comparative study of submicron particle sizing platforms: Accuracy, precision and resolution analysis of polydisperse particle size distributions," *Journal of Colloid and Interface Science*, vol. 405, pp. 322–330, Sep. 2013, doi: 10.1016/j.jcis.2013.02.030.

[53] C. Montis *et al.*, "Size distribution of extracellular vesicles by optical correlation techniques," *Colloids and Surfaces B: Biointerfaces*, vol. 158, Oct. 2017, doi: 10.1016/j.colsurfb.2017.06.047.

[54] C. A. Siedlecki, I. Wen Wang, J. M. Higashi, K. Kottke-Marchant, and R. E. Marchant, "Platelet-derived microparticles on synthetic surfaces observed by atomic force microscopy and fluorescence microscopy," *Biomaterials*, vol. 20, no. 16, pp. 1521–1529, Aug. 1999, doi: 10.1016/S0142-9612(99)00065-4.

[55] Y. Yuana *et al.*, "Atomic force microscopy: a novel approach to the detection of nanosized blood microparticles," *Journal of Thrombosis and Haemostasis*, vol. 8, no. 2, pp. 315–323, Feb. 2010, doi: 10.1111/j.1538-7836.2009.03654.x.

[56] R. A. Dragovic *et al.*, "Sizing and phenotyping of cellular vesicles using Nanoparticle Tracking Analysis," *Nanomedicine: Nanotechnology, Biology and Medicine*, vol. 7, no. 6, pp. 780–788, Dec. 2011, doi: 10.1016/j.nano.2011.04.003.

[57] U. Erdbrügger and J. Lannigan, "Analytical challenges of extracellular vesicle detection: A comparison of different techniques," *Cytometry Part A*, vol. 89, no. 2, pp. 123–134, Feb. 2016, doi: 10.1002/cyto.a.22795.

[58] C. M. Hoo, N. Starostin, P. West, and M. L. Mecartney, "A comparison of atomic force microscopy (AFM) and dynamic light scattering (DLS) methods to characterize nanoparticle size distributions," *Journal of Nanoparticle Research*, vol. 10, no. S1, pp. 89–96, Dec. 2008, doi: 10.1007/s11051-008-9435-7.

[59] E. van der Pol, F. Coumans, Z. Varga, M. Krumrey, and R. Nieuwland, "Innovation in detection of microparticles and exosomes," *Journal of Thrombosis and Haemostasis*, vol. 11, Jun. 2013, doi: 10.1111/jth.12254.

[60] L. Doyle and M. Wang, "Overview of Extracellular Vesicles, Their Origin, Composition, Purpose, and Methods for Exosome Isolation and Analysis," *Cells*, vol. 8, no. 7, p. 727, Jul. 2019, doi: 10.3390/cells8070727.

[61] S. Grimnes and Ø. G. Martinsen, "Selected Applications," in *Bioimpedance and Bioelectricity Basics*, Elsevier, 2015, pp. 405–494. doi: 10.1016/B978-0-12-411470-8.00010-6.

[62] L. Luo, S. R. German, W.-J. Lan, D. A. Holden, T. L. Mega, and H. S. White, "Resistive-Pulse Analysis of Nanoparticles," *Annual Review of Analytical Chemistry*, vol. 7, no. 1, pp. 513–535, Jun. 2014, doi: 10.1146/annurev-anchem-071213-020107.

[63] T. Ito, L. Sun, R. R. Henriquez, and R. M. Crooks, "A Carbon Nanotube-Based Coulter Nanoparticle Counter," *Accounts of Chemical Research*, vol. 38, no. 8, pp. 687–687, Aug. 2005, doi: 10.1021/ar050133v.

[64] Y. Song, J. Zhang, and D. Li, "Microfluidic and Nanofluidic Resistive Pulse Sensing: A Review," *Micromachines*, vol. 8, no. 7, p. 204, Jun. 2017, doi: 10.3390/mi8070204.

[65] G. M. Whitesides, "The origins and the future of microfluidics," *Nature*, vol. 442, no. 7101, pp. 368–373, Jul. 2006, doi: 10.1038/nature05058.

[66] C. D. Chin, V. Linder, and S. K. Sia, "Commercialization of microfluidic point-of-care diagnostic devices," *Lab on a Chip*, vol. 12, no. 12, p. 2118, 2012, doi: 10.1039/c2lc21204h.

[67] G. Choi, E. Murphy, and W. Guan, "Microfluidic Time-Division Multiplexing Accessing Resistive Pulse Sensor for Particle Analysis," *ACS Sensors*, vol. 4, no. 7, pp. 1957–1963, Jul. 2019, doi: 10.1021/acssensors.9b01067.

[68] E. Garza-Licudine, D. Deo, S. Yu, A. Uz-Zaman, and W. B. Dunbar, "Portable nanoparticle quantization using a resizable nanopore instrument - The IZON qNano™," Aug. 2010. doi: 10.1109/IEMBS.2010.5627861.

[69] E. Weatherall and G. R. Willmott, "Applications of tunable resistive pulse sensing," *The Analyst*, vol. 140, no. 10, 2015, doi: 10.1039/C4AN02270J.

[70] K. Misiunas, N. Ermann, and U. F. Keyser, "QuipuNet: Convolutional Neural Network for Single-Molecule Nanopore Sensing," *Nano Letters*, vol. 18, no. 6, pp. 4040–4045, Jun. 2018, doi: 10.1021/acs.nanolett.8b01709.

[71] W. L. Chandler, W. Yeung, and J. F. Tait, "A new microparticle size calibration standard for use in measuring smaller microparticles using a new flow cytometer," *Journal of*

Thrombosis and Haemostasis, vol. 9, no. 6, pp. 1216–1224, Jun. 2011, doi: 10.1111/j.1538-7836.2011.04283.x.

[72] M. Sivakumaran and M. Platt, "Tunable resistive pulse sensing: potential applications in nanomedicine," *Nanomedicine*, vol. 11, no. 16, Aug. 2016, doi: 10.2217/nnm-2016-0097.

[73] E. Serrano-Pertierra *et al.*, "Extracellular Vesicles: Current Analytical Techniques for Detection and Quantification," *Biomolecules*, vol. 10, no. 6, p. 824, May 2020, doi: 10.3390/biom10060824.

[74] Y. Yu *et al.*, "Electrical and Label-Free Quantification of Exosomes with a Reduced Graphene Oxide Field Effect Transistor Biosensor," *Analytical Chemistry*, vol. 91, no. 16, pp. 10679–10686, Aug. 2019, doi: 10.1021/acs.analchem.9b01950.

[75] S. Wang *et al.*, "Aptasensor with Expanded Nucleotide Using DNA Nanotetrahedra for Electrochemical Detection of Cancerous Exosomes," *ACS Nano*, vol. 11, no. 4, pp. 3943–3949, Apr. 2017, doi: 10.1021/acsnano.7b00373.

[76] C. Wen, S. Li, S. Zeng, Z. Zhang, and S.-L. Zhang, "Autogenic analyte translocation in nanopores," *Nano Energy*, vol. 60, Jun. 2019, doi: 10.1016/j.nanoen.2019.03.092.

[77] E. L. C. J. Blundell, L. J. Mayne, E. R. Billinge, and M. Platt, "Emergence of tunable resistive pulse sensing as a biosensor," *Analytical Methods*, vol. 7, no. 17, 2015, doi: 10.1039/C4AY03023K.

[78] W. Anderson, R. Lane, D. Korbie, and M. Trau, "Observations of Tunable Resistive Pulse Sensing for Exosome Analysis: Improving System Sensitivity and Stability," *Langmuir*, vol. 31, no. 23, Jun. 2015, doi: 10.1021/acs.langmuir.5b01402.

[79] W. M. Parkin and M. Drndić, "Signal and Noise in FET-Nanopore Devices," *ACS Sensors*, vol. 3, no. 2, Feb. 2018, doi: 10.1021/acssensors.7b00708.

[80] P. Dutta and P. M. Horn, "Low-frequency fluctuations in solids: 1/f noise," *Reviews of Modern Physics*, vol. 53, no. 3, Jul. 1981, doi: 10.1103/RevModPhys.53.497.

[81] A. J. W. Hartel, S. Shekar, P. Ong, I. Schroeder, G. Thiel, and K. L. Shepard, "High bandwidth approaches in nanopore and ion channel recordings - A tutorial review," *Analytica Chimica Acta*, vol. 1061, Jul. 2019, doi: 10.1016/j.aca.2019.01.034.

[82] D. Kozak, W. Anderson, R. Vogel, and M. Trau, "Advances in resistive pulse sensors: Devices bridging the void between molecular and microscopic detection," *Nano Today*, vol. 6, no. 5, Oct. 2011, doi: 10.1016/j.nantod.2011.08.012.

[83] S. Akhtarian, S. Miri, A. Doostmohammadi, S. K. Brar, and P. Rezai, "Nanopore sensors for viral particle quantification: current progress and future prospects," *Bioengineered*, vol. 12, no. 2, pp. 9189–9215, Dec. 2021, doi: 10.1080/21655979.2021.1995991.

[84] B. J. Kenner, V. L. W. Go, S. T. Chari, A. E. Goldberg, and L. J. Rothschild, "Early Detection of Pancreatic Cancer," *Pancreas*, vol. 46, no. 10, pp. 1238–1241, Nov. 2017, doi: 10.1097/MPA.0000000000000939.

[85] L. Rahib, B. D. Smith, R. Aizenberg, A. B. Rosenzweig, J. M. Fleshman, and L. M. Matrisian, "Projecting Cancer Incidence and Deaths to 2030: The Unexpected Burden of Thyroid, Liver, and Pancreas Cancers in the United States," *Cancer Research*, vol. 74, no. 11, pp. 2913–2921, Jun. 2014, doi: 10.1158/0008-5472.CAN-14-0155.

[86] B. Costa-Silva *et al.*, "Pancreatic cancer exosomes initiate pre-metastatic niche formation in the liver," *Nature Cell Biology*, vol. 17, no. 6, pp. 816–826, Jun. 2015, doi: 10.1038/ncb3169.

[87] Y. Tai, K. Chen, J. Hsieh, and T. Shen, "Exosomes in cancer development and clinical applications," *Cancer Science*, vol. 109, no. 8, pp. 2364–2374, Aug. 2018, doi: 10.1111/cas.13697.

[88] T. Lener *et al.*, "Applying extracellular vesicles based therapeutics in clinical trials – an ISEV position paper," *Journal of Extracellular Vesicles*, vol. 4, no. 1, p. 30087, Jan. 2015, doi: 10.3402/jev.v4.30087.

[89] S. P. Nana-Sinkam, M. Acunzo, C. M. Croce, and K. Wang, "Extracellular Vesicle Biology in the Pathogenesis of Lung Disease," *American Journal of Respiratory and Critical Care Medicine*, vol. 196, no. 12, pp. 1510–1518, Dec. 2017, doi: 10.1164/rccm.201612-2457PP.

[90] E. H. Koritzinsky, J. M. Street, R. A. Star, and P. S. T. Yuen, "Quantification of Exosomes," *Journal of Cellular Physiology*, vol. 232, no. 7, pp. 1587–1590, Jul. 2017, doi: 10.1002/jcp.25387.

[91] F. A. W. Coumans *et al.*, "Reproducible extracellular vesicle size and concentration determination with tunable resistive pulse sensing," *Journal of Extracellular Vesicles*, vol. 3, no. 1, p. 25922, Jan. 2014, doi: 10.3402/jev.v3.25922.

[92] C. Afilipoaei and H. Teodorescu-Draghicescu, "A Review over Electromagnetic Shielding Effectiveness of Composite Materials," in *The 14th International Conference on Interdisciplinarity in Engineering—INTER-ENG 2020*, Dec. 2020, p. 23. doi: 10.3390/proceedings2020063023.

[93] S. Kumar and H. P. Lee, "Recent Advances in Acoustic Metamaterials for Simultaneous Sound Attenuation and Air Ventilation Performances," *Crystals*, vol. 10, no. 8, p. 686, Aug. 2020, doi: 10.3390/cryst10080686.

[94] D. Sun *et al.*, "Dye-free spectrophotometric measurement of nucleic acid-to-protein ratio for cell-selective extracellular vesicle discrimination," *Biosensors and Bioelectronics*, vol. 179, p. 113058, May 2021, doi: 10.1016/j.bios.2021.113058.

[95] K. Rasuleva *et al.*, "β-Sheet Richness of the Circulating Tumor-Derived Extracellular Vesicles for Noninvasive Pancreatic Cancer Screening," *ACS Sensors*, vol. 6, no. 12, pp. 4489–4498, Dec. 2021, doi: 10.1021/acssensors.1c02022.

[96] X. Wu, Y. Kang, Y.-N. Wang, D. Xu, D. Li, and D. Li, "Microfluidic differential resistive pulse sensors," *Electrophoresis*, Jun. 2008, doi: 10.1002/elps.200700912.

[97] Y. Pei, R. Vogel, and C. Minelli, "Tunable resistive pulse sensing (TRPS)," in *Characterization of Nanoparticles*, Elsevier, 2020, pp. 117–136. doi: 10.1016/B978-0-12-814182-3.00009-2.

[98] S. L. N. Maas, M. L. D. Broekman, and J. de Vrij, "Tunable Resistive Pulse Sensing for the Characterization of Extracellular Vesicles," 2017, pp. 21–33. doi: 10.1007/978-1-4939-6728-5_2.

[99] G. Goyal, K. J. Freedman, and M. J. Kim, "Gold Nanoparticle Translocation Dynamics and Electrical Detection of Single Particle Diffusion Using Solid-State Nanopores," *Analytical Chemistry*, vol. 85, no. 17, pp. 8180–8187, Sep. 2013, doi: 10.1021/ac4012045.

[100] E. R. Billinge and M. Platt, "Multiplexed, label-free detection of biomarkers using aptamers and Tunable Resistive Pulse Sensing (AptaTRPS)," *Biosensors and Bioelectronics*, vol. 68, pp. 741–748, Jun. 2015, doi: 10.1016/j.bios.2015.02.011.

[101] G. Choi, E. Murphy, and W. Guan, "Time-division multiplexed resistive pulse sensor on a microfluidic chip," in *2019 IEEE SENSORS*, Oct. 2019, pp. 1–4. doi: 10.1109/SENSORS43011.2019.8956766.

[102] B. Yan, H. Cui, J. Zhou, and H. Wang, "Electrical Noises Reduction in Nanopores Experiments Based on Consensus Filter," *Química Nova*, 2020, doi: 10.21577/0100-4042.20170560.

[103] G. Rempfer, S. Ehrhardt, C. Holm, and J. de Graaf, "Nanoparticle Translocation through Conical Nanopores: A Finite Element Study of Electrokinetic Transport," *Macromolecular Theory and Simulations*, vol. 26, no. 1, p. 1600051, Jan. 2017, doi: 10.1002/mats.201600051.

[104] S. R. German, L. Luo, H. S. White, and T. L. Mega, "Controlling Nanoparticle Dynamics in Conical Nanopores," *The Journal of Physical Chemistry C*, vol. 117, no. 1, pp. 703–711, Jan. 2013, doi: 10.1021/jp310513v.